

ANTI-SWING CONTROLLER OF 3D CRANE

By

GILLIAN KHINAH SYLVESTER

FINAL PROJECT REPORT

Submitted to the Electrical & Electronics Engineering Programme
in Partial Fulfillment of the Requirements
for the Degree
Bachelor of Engineering (Hons)
(Electrical & Electronics Engineering)

Universiti Teknologi Petronas
Bandar Seri Iskandar
31750 Tronoh
Perak Darul Ridzuan

© Copyright 2006

by

Gillian Khinah Sylvester, 2006

CERTIFICATION OF APPROVAL

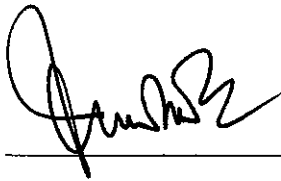
ANTI-SWING CONTROLLER OF 3D CRANE

by

Gillian Khinah Sylvester

A project dissertation submitted to the
Electrical & Electronics Engineering Programme
Universiti Teknologi PETRONAS
in partial fulfilment of the requirement for the
Bachelor of Engineering (Hons)
(Electrical & Electronics Engineering)

Approved:



A.P. Dr. Mohd Noh b. Karsiti
Project Supervisor

UNIVERSITI TEKNOLOGI PETRONAS
TRONOH, PERAK

June 2006

CERTIFICATION OF ORIGINALITY

This is to certify that I am responsible for the work submitted in this project, that the original work is my own except as specified in the references and acknowledgements, and that the original work contained herein have not been undertaken or done by unspecified sources or persons.



Gillian Khinah Sylvester

ABSTRACT

Crane control is frequently studied where anti-swing control of the load has been one of the important issues. It is important to have anti-swing control for a crane because the swing motion of the suspended payload results in many problems to the productivity and safety. Modeling and control of a crane is a long-time research interest. Many researchers have worked on this issue of anti-swing control of the crane system. Their work can be divided into largely two groups: open loop and closed loop control. This project focuses on the development of anti-swing control for the crane. Several controllers will be studied, let it be open loop system and closed loop system for the anti-swing control. The simulation of the 3DCrane is done using MATLAB and RTWT toolbox package. This report detailed the mathematical modelling of the crane system and the model verification. The model of the crane system is developed using Lagrangian dynamics and electromechanical theory. In this report it is shown that a crane system can be represented as two sub models which are coupled by a term which includes the rope length as a parameter. The model is verified as an accurate model of a crane system and it is used to simulate performance of controllers using Matlab. Two types of controllers have been designed in this project which is PD controller and full state feedback (FSF) using pole placement method. The performance of the controllers is discussed and it is proven that the controllers have given a good control on the position of the cart and reduces the swing of the load.

ACKNOWLEDGEMENTS

This project would not have been possible without the assistance and guidance of certain individuals whose contributions have helped in its completion.

First of all I would like to up lift my utmost gratitude and thanks to God for the spirit of wisdom, knowledge and understanding He has poured on me. For the strength and faith He provides me that I am able to go through every single circumstances and problems throughout the project,

Also I would like to record my sincere thanks and utmost appreciation to the project supervisor, A.P.Dr. Mohd. Noh Karsiti, for his valuable input, guidance and understanding at all times throughout the study and development.

Not forgotten, I would like to express heartiest gratitude to Mr. Azhar and Mr. Jurimi, the technicians and my colleagues for their help and support during the project, and my family for their advice and prayers that strengthens me.

Lastly, I would like to thank all persons who have contributed to this project in one way or another but have been inadvertently not been.

TABLE OF CONTENTS

LIST OF TABLES	ix
LIST OF FIGURES.....	x
CHAPTER 1 INTRODUCTION	1
1.1 Background of Study.....	1
1.2 Problem Statement	1
1.2.1 Problem Identification	1
1.2.2 Significance of the project	2
1.3 Scope of Study and Objectives.....	2
1.3.1 Scope of Study	2
1.3.2 Objectives	3
CHAPTER 2 LITERATURE REVIEW AND THEORY	4
2.1 Literature Review	4
2.2 Theory	6
2.2.1 A simple crane system	6
2.2.2 The Lagrangian	8
The Lagrangian of the pendulum	9
Equations of motion	10
Pendulum--Equations of motion	10
CHAPTER 3 METHODOLOGY & PROJECT WORK	12
3.1 Procedure Identification	12
3.2 Tools Required	13
3.2.1 Tools	13
3.2.2 Software	13
3.3 Experiment Procedures.....	13
CHAPTER 4 RESULTS & DISCUSSION.....	18
4.1 Results	18
4.1.1 Conceptual Study with Overhead Crane (Open Loop System Response).....	18
4.1.2 Mathematical Modelling of the cart and swing dynamic and DC motor	19
4.1.3 Model Verification.....	33
4.1.4 PD Controller.....	37

.....	38
4.1.5 Full State Feedback Using Pole Placement Method (FSF)....	43
4.2 Discussion	44
4.2.1 Conceptual Study with Overhead Crane (System Description)	44
4.2.2 Mathematical Modelling of the cart and swing dynamic and DC motor	47
4.2.3 PD Controller.....	49
4.2.4 Full State Feedback (FSF) using Pole Placement Method	50
CHAPTER 5 CONCLUSION & RECOMMENDATION	52
REFERENCES.....	53
APPENDICES.....	55
Appendix A Milestone of Second Semester of Final Year Project.....	56
Appendix B Matlab file for controller.....	58
Appendix C Simulink Diagram for Model Verification	60

LIST OF TABLES

Table 1 Ziegler-Nichols Tuning Rule Based on Critical Gain, K_{cr} and Critical Period, P_{cr} (Second method)	15
Table 2 Procedure for hand tuning a PID controller.	16
Table 3 Values of the parameters (x-direction).....	35
Table 4 Values of the parameters (z-direction).....	36
Table 5 PD constant values for x-direction and z-direction.....	42

CHAPTER 1

INTRODUCTION

1.1 Background of Study

The title of this final year project is anti-swing controller of a 3Dcrane. The main focus of this topic is to study the types of controller to reduce swing motion of the load which is connected to the cart of the crane. The hardware that is used is 3D crane which is a laboratory model for an industrial crane. Cranes are used in numerous industrial applications, such as loading and unloading of containers, nuclear waste handling facilities, factory automation and basically in any industries which requires heavy goods to be lifted and moved. In most of these places the productivity of the activities depends on how efficiently the crane is managed. Moreover, these cranes are being used for 24 hours a day because even a short down time greatly affects the operations of the plant.

1.2 Problem Statement

1.2.1 Problem Identification

Regardless of any crane's specific design, the physics of a load suspended from a cable introduces an inherent problem: payload swinging. A weight suspended on a long string or cables acts very much like a pure pendulum. The movement of a construction crane or gust of wind may excite a suspended payload into oscillations such as the movement of a pendulum. In a frictionless environment, once the weight is offset from the vertical, it will swing back to a point just as far on the other side and keep doing that forever. This complies with the Newton's first law of motion, which states that it is the tendency of a body to maintain its state of uniform motion unless acted on by an external force.

The swing motion results in direct loss, the cost of which is realized by lost performance such as delays to critically linked activities, damage to materials, and liability associated with accidents. The swing motion of the load often limits its operational efficiency and safety. A lot of time is lost by crane operators in trying to bring the load connected to the crane to a standstill. The swing occurring in the load also prevents the operator to run the crane at its maximum speed. Thus, the need to control or reduce this swing motion is studied and it has drawn the interest of control engineers for a long time.

1.2.2 Significance of the project

As stated earlier, the anti-swing controller is needed to control or reduce the swing motion of payload of the crane. In this study the mathematical model of the crane is derived. From the model, a controller is designed and implemented in order to control the position of the cart and reduce the swinging motion of the payload.

1.3 Scope of Study and Objectives

1.3.1 Scope of Study

The aim of this project is to develop and investigate an anti-swing controller that would cancel the swing oscillations. The scope of study is to analyse the swing motion of a payload suspended from a crane in x-direction. The mathematical model of the pendulum is developed and verified, and a methodology is developed for the testing of the controllers. The project is in the form of laboratory experiments, modeling, simulations and analysis of the controller. A controller that can control the cart position and reduce the swing oscillation is designed.

1.3.2 Objectives

The following objectives are set out in order to achieve the aim of this project.

- 1) The modeling of the crane based on Lagrangian and electromechanical theory – a mathematical model of the crane system is derived to have the same performance as the real-time system
- 2) To design and implement the controller for cart positioning and swing cancellation

CHAPTER 2

LITERATURE REVIEW AND THEORY

2.1 Literature Review

Modeling and control of a crane is a long-time research interest. Different industrial applications require different crane control systems. Some applications require fast traversal time and optimization of the cart's motion is required. Others require very little or no swing of the goods as they are being moved. Some others require that all three dynamics of the crane be optimally controlled such as the load positioning swing cancellations and load height.

Many researchers have worked on this issue of anti-swing control of the crane system. These controllers consist of, but are not limited to linear, non-linear, adaptive and multivariable controllers. Thus, the solution to the control of the gantry crane is not limited to one specific area of control theory. By observing the performance of different classes of controllers, improvements in the control of industrial gantry cranes may be achieved. Their work can be divided into largely two groups: open loop and closed loop control.

The open loop methods, such as low pass filter, symmetric acceleration profile [1], and input shaping [2][3], are intended not to excite the swing motion. They are simple to implement but cannot suppress swing motion caused by external disturbances. They also do not perform satisfactorily for a wide range of payloads.

The disadvantages of open-loop systems, namely sensitivity to disturbances and inability to correct for these disturbances, may be overcome in closed loop system [4].

The closed loop system compensated for disturbances by measuring the output response, feeding that measurement back through a feedback path and comparing that response to the input at the summing junction. The closed loop method of swing motion provides the ability to eliminate existing swing motion and rejects disturbances at the cost of extra sensor. Many closed loop controller have been studied. Some of the closed loop controllers are based on root locus, loop-shaping, LQR method and feedback linearization.

A method of using feedforward anti-sway control has been attempted [5]. The applied method is the one that calculates the trolley travel pattern to stop swaying, in advance and that the calculated pattern is combined with the feedback control. Ho-Hoon Lee et al. [6] developed a closed-loop controller based on root locus and loop-shaping. He also derived a near dynamic model of a three-dimensional overhead crane based on two degree of freedom swing angle. Wen. B et al. [7] developed the closed-loop controller based on the LQR method. This approach also requires the knowledge of the payloads beforehand. Ji Sup Yoon et al [8] designed several anti-swing controllers using both open-loop and closed-loop approaches. In order to develop more effective and robust controller he developed a pre-programmed feedback controller and a fuzzy controller. He implemented all the controllers on a one-directional linear pilot crane system.

2.2 Theory

2.2.1 A simple crane system

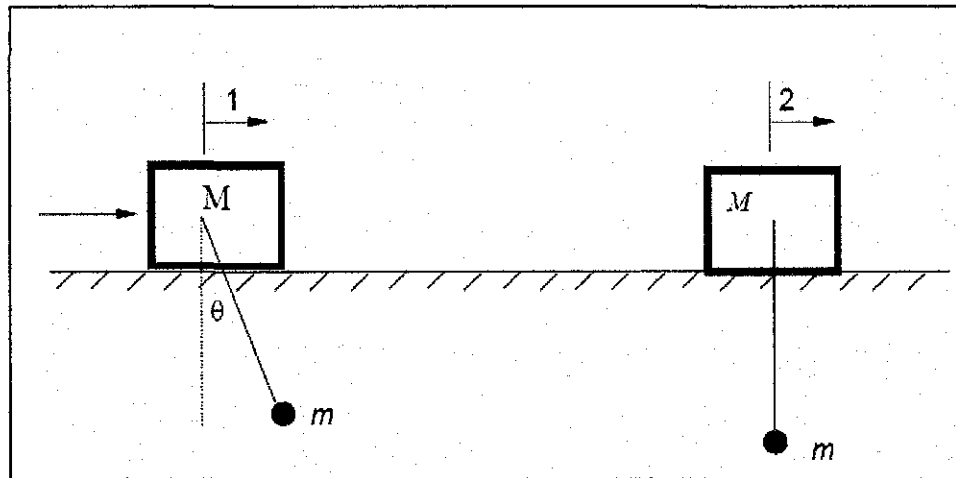


Figure 1 A Simple overhead crane system

A simple overhead crane system, shown in Figure 1, consists of a cart of M , and a pendulum with payload, m . The control objective is to move the cart from position '1' to position '2' with minimum or possibly zero swing angle, θ .

When an undisturbed payload is suspended from a crane, at it resides at its stable equilibrium, vertically beneath the tip of the boom. A perturbation, such as movement of the crane or a gust of wind provides a form of kinetic energy which displaces the payload from its stable equilibrium. As the payload moves from its lowest position, it gains potential energy in the form of vertical displacement. This continues until all the kinetic energy has been transformed into potential energy, and the payload achieves an oscillation peak.

Next, conservation of mechanical energy forces the displaced payload to reduce its potential energy by swinging to its lowest position. This motion provides the payload with the momentum, which carries the payload to an oscillation peak on the opposite side of the stable equilibrium. The pendulum-like motion will continue as an oscillation or vibration, with a measurable frequency, f . Various damping forces

acting on the system will gradually reduce the magnitude of the oscillation peaks, eventually stopping the motion.

A simple pendulum is one which can be considered to be a point mass suspended from a string or rod of negligible mass. It is resonant system with a single resonant frequency. For small amplitudes, the period of such a pendulum can be approximated by:

$$T = 2\pi\sqrt{\frac{L}{g}}$$

The motion of a simple pendulum is like simple harmonic motion in that the equation for the angular displacement is

$$\theta = \theta_{\max} \sin \sqrt{\frac{g}{L}}t$$

which is the same form as the motion of a mass on a spring:

$$y = A \sin \sqrt{\frac{k}{m}}t$$

The angular frequency of the motion is then given by $\omega = \sqrt{\frac{g}{L}}$ compared to $\omega = \sqrt{\frac{k}{m}}$ for a mass on a spring. The frequency of the pendulum in Hz is given by

$$f = \frac{1}{2\pi} \sqrt{\frac{g}{L}} \text{ and the period of the motion is then } T = 2\pi \sqrt{\frac{L}{g}}.$$

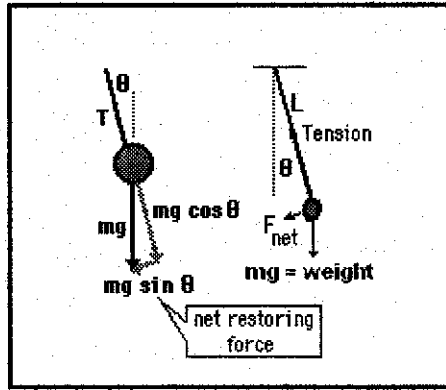


Figure 2 Simple pendulum

A point mass hanging on a massless string is an idealized example of a simple pendulum. When displaced from its equilibrium point, the restoring force which brings it back to the center is given by:

$$F_{net} = -mg \sin \theta$$

For small angles θ , we can use the approximation $\sin \theta = \theta$ in which case Newton's 2nd law takes the form $ma = -mg\theta$. Even in this approximate case, the solution of the equation uses calculus and differential solutions. The differential equation is

$$\frac{d^2\theta}{dt^2} + \frac{g}{L}\theta = 0 \text{ and for small angles } \theta \text{ the solution is } \theta \cong \theta_{\max} \sin \sqrt{\frac{g}{L}}t.$$

2.2.2 The Lagrangian

According to [9], Lagrangian mechanics is mathematically equivalent to the usual Newtonian approach of "apply forces to things and see how they move". Instead of examining the forces on a body directly, it looks at the kinetic and potential energies of a system of objects. This approach simplifies many complicated problems. In Lagrangian mechanics we start by writing down the Lagrangian of the system

$$L=T-U$$

where T is the kinetic energy and U is the potential energy. Both are expressed in terms of coordinates (q, \dot{q}) where $q \in \mathbb{R}^n$ is the position vector and $\dot{q} \in \mathbb{R}^n$ is the velocity vector.

The Lagrangian of the pendulum

An example is the physical pendulum (see Figure 2.3).

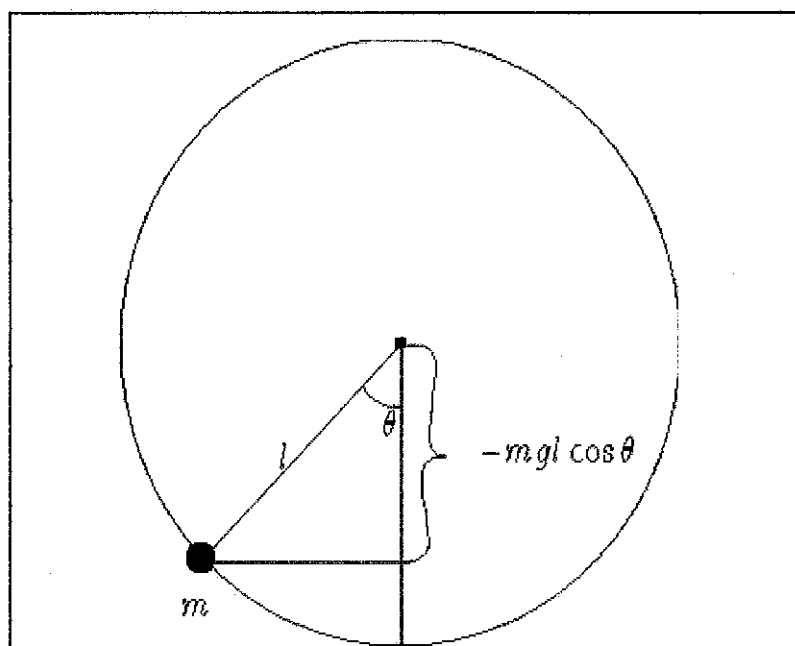


Figure 3 The configuration space of the pendulum

The natural configuration space of the pendulum is the circle. The natural coordinate on the configuration space is the angle θ . If the mass of the ball is m and the length of the rod is l then we have

$$T = \frac{1}{2}m(l\dot{\theta})^2$$

$$U = -mgl \cos \theta$$

Thus, the Lagrangian in coordinates $(\theta, \dot{\theta})$ is

$$L = \frac{1}{2}m(l\dot{\theta})^2 + mgl \cos \theta$$

Equations of motion

In Lagrangian mechanics the equations of motion are written in the following universal form:

$$\frac{d}{dt} \left(\frac{\partial L}{\partial \dot{q}} \right) = \frac{\partial L}{\partial q}$$

Pendulum--Equations of motion

For example, for the pendulum we have:

$$\frac{\partial L}{\partial \dot{\theta}} = ml^2 \dot{\theta}$$

$$\frac{\partial L}{\partial \theta} = -mgl \sin \theta$$

Thus, the equations of motion are written as

$$\frac{d}{dt} (ml^2 \dot{\theta}) = -mgl \sin \theta$$

This equation can be written as second order equation

$$ml^2 \ddot{\theta} = -mgl \sin \theta$$

or in the traditional way

$$\ddot{\theta} = -\frac{g}{l} \sin \theta$$

Meaning of Dot

We should emphasize that $\dot{\theta}$ has dual meaning. It is both a coordinate and the derivative of the position. This traditional abuse of notation should be resolved in favor of one of these interpretations in every particular situation.

CHAPTER 3

METHODOLOGY & PROJECT WORK

3.1 Procedure Identification

The procedures involved in completing this project are shown as below in Figure 4.

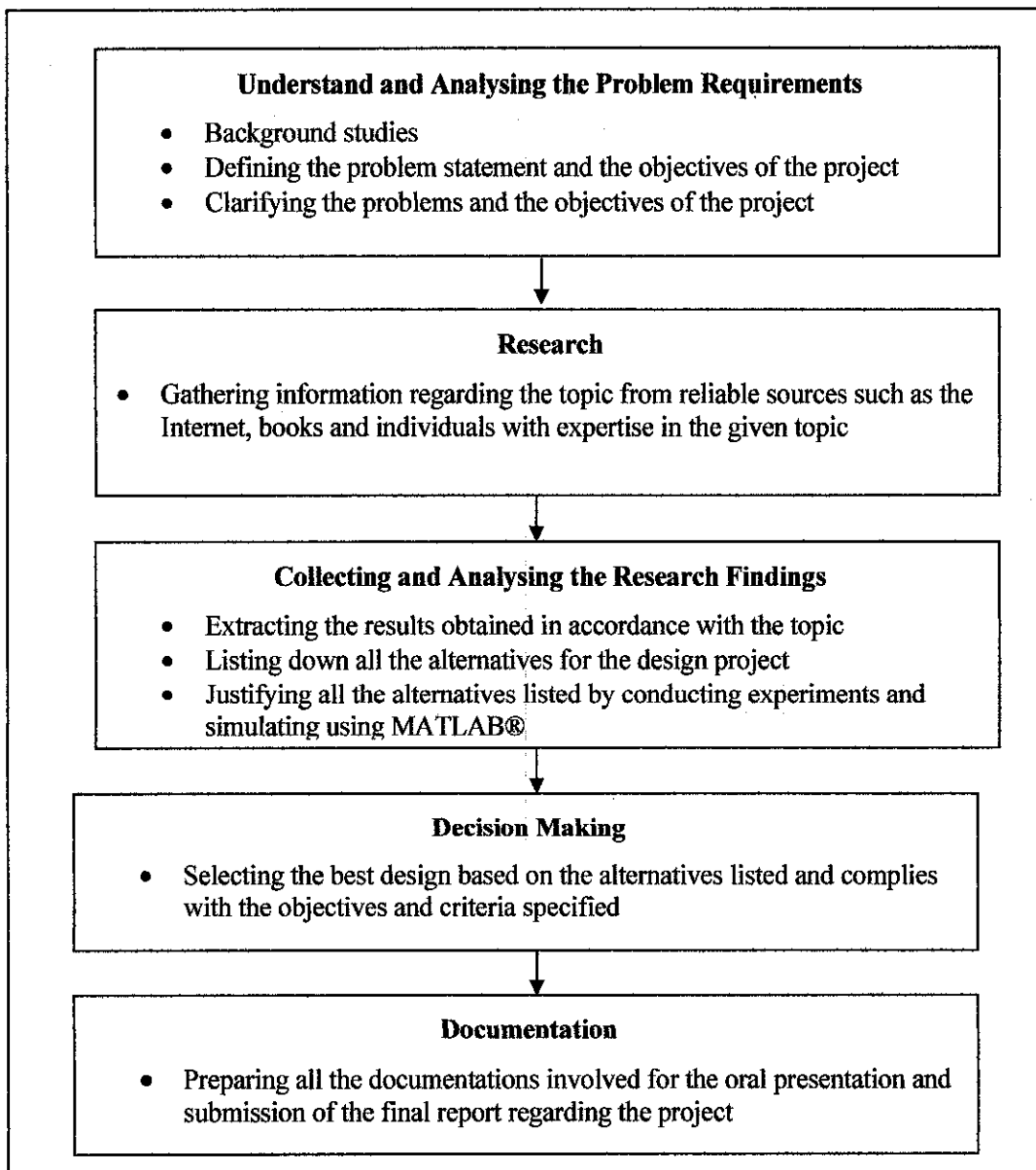


Figure 4 Flowchart for procedure

3.2 Tools Required

3.2.1 Tools

The **3DCrane** is a laboratory model for an industrial crane. It is a non-linear electromechanical system having complex dynamic behavior. The control of the crane in various modes is achieved under MS Windows® NT using Matlab/Simulink and RTWT toolbox package. The 3DCrane consists of a payload hanging on a pendulum-like lift-line wound by a motor wound on a cart.

3.2.2 Software

MATLAB®/Simulink® environment and **RTWT** toolbox package is used to design and generate real-time controller. It contains the library of ready-to use real-time controllers. This software will be used to simulate the controller to reduce the swing motion of the load.

3.3 Experiment Procedures

This section develops the methods to setup the test bed and calibrate the equipments. The 3DCrane setup consists of a payload hanging on a pendulum-like lift-line wound by a motor mounted on a cart. It also consists of IBM Compatible PC, RT-DAC/PCI, Inteco 3DCrane System consisting of 3DCrane Mechanical Unit and 3DCran Interface Unit. . This experiment is basically to ensure that the setup of the 3DCrane is correct. This can be done by having the output of the cart's position and payload's angle without actual input. The position of the cart and the payload's angle are set manually.

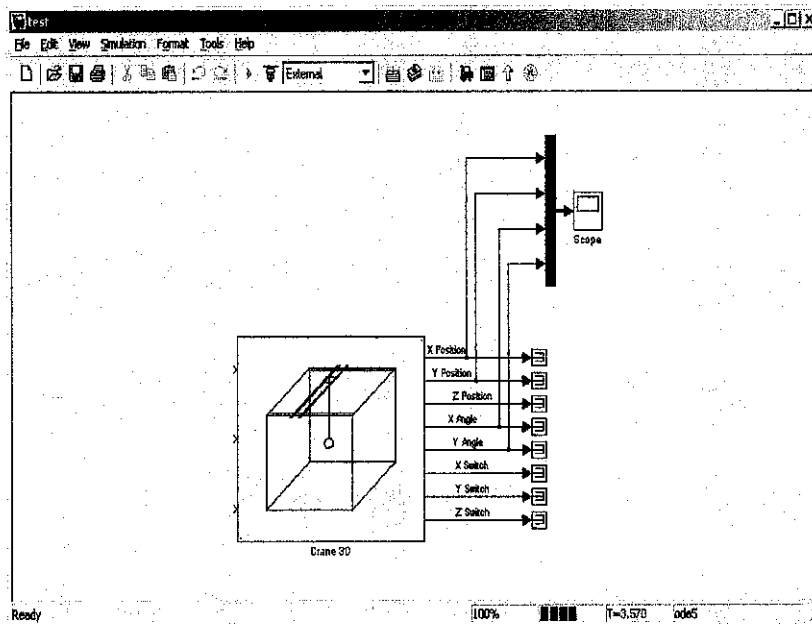


Figure 5 Simulink Block for Experiment 1

The next experiment is on the model verification. Model verification has been performed in order to validate the derived dynamic model of the system. For the same input to the system, the outputs from the derived dynamic model are compared with the outputs from the real-time system. Firstly, the verification of the DC motor, cart and swing dynamics are done. The parameters that were determined include the length of the lift-line, the mass of the cart and load and the motor constant. Secondly, the verification of the hoist is carried out. The parameters that were determined include the motor constant and the mass of the load. All the results are to be kept for analysis.

The next experiment is to design the controller for the 3DCrane. This controller controls the cart position and the swing motion of the load. The controller that was designed is PD controller.

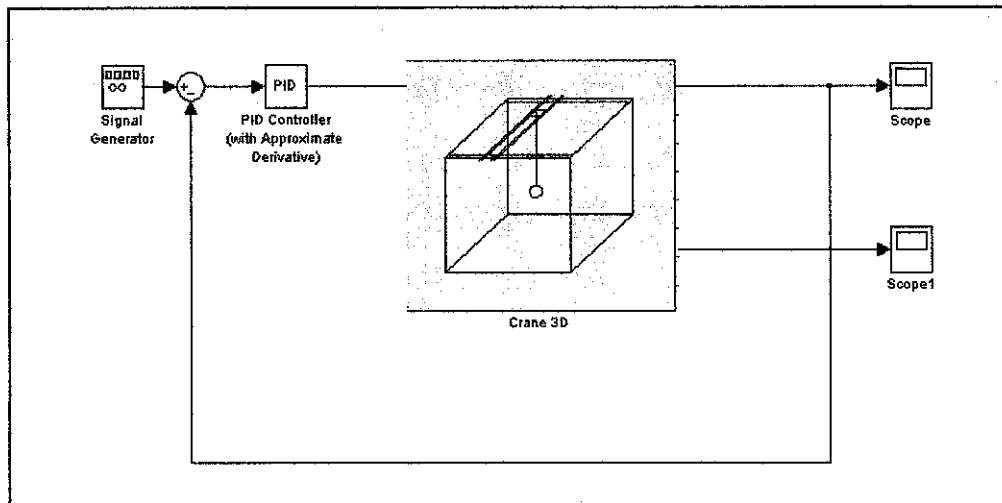


Figure 6 Simulink diagram of the system with PD controller

Ziegler and Nichols proposed rules for determining values of the proportional gain K_p , integral time T_i , and derivative time T_d based on the transient response characteristics of a given plant [13]. In this project, the second method of the Z-N tuning rule is used. Using the proportional control action only, the K_p is increased from 0 to critical value K_{cr} at which the output first exhibit sustained oscillations. Other alternative is using the Routh table to determine the K_{cr} . Thus the critical gain K_{cr} and the corresponding period P_{cr} are experimentally determined. Ziegler and Nichols suggested that the values of the parameters K_p , T_i and T_d are set according to the formula shown in Table 1.

Table 1 Ziegler-Nichols Tuning Rule Based on Critical Gain, K_{cr} and Critical Period, P_{cr} (Second method)¹

Type of controller	K_p	T_i	T_d
P	$0.5 K_{cr}$	inf	0
PI	$0.45 K_{cr}$	$1/1.2 P_{cr}$	0
PID	$0.6 K_{cr}$	$0.5 P_{cr}$	$0.125 P_{cr}$

¹ Table from Katsuhiko Ogata, *Modern Control Engineering*, Second Edition.

Another convenient method to hand-tune the gains in a PID controller is explained by Jan Jantzen in [10]. This method is in four steps, which are shown in Table 1 below. Although the hand tuning procedure is made for a PID controller it can be also easily be used to tune a PD controller by only skipping step 4. The hand tuning procedure is carried out two times, once for the cart's position controller and then for the pendulum's angle controller.

Table 2 Procedure for hand tuning a PID controller².

Step 1 :	Remove all integral and derivative by setting $T_d=0$ and $I/T_i=0$.
Step 2:	Tune the proportional gain K_p to give the desired response, ignoring any final value offset from the setpoint.
Step 3:	Increase the proportional gain further and adjust the derivative gain T_d to dampen the overshoot.
Step 4:	Adjust the integral gain I/T_i to remove any final value offset.
Step 5:	Repeat until the proportional gain K_p is as large as possible.

² Table from J. Jantzen, *Tuning of Fuzzy PID Controllers*, Tech. Rept no 98-H 871, 16 April 1999, Technical University of Denmark, Department of Automation.

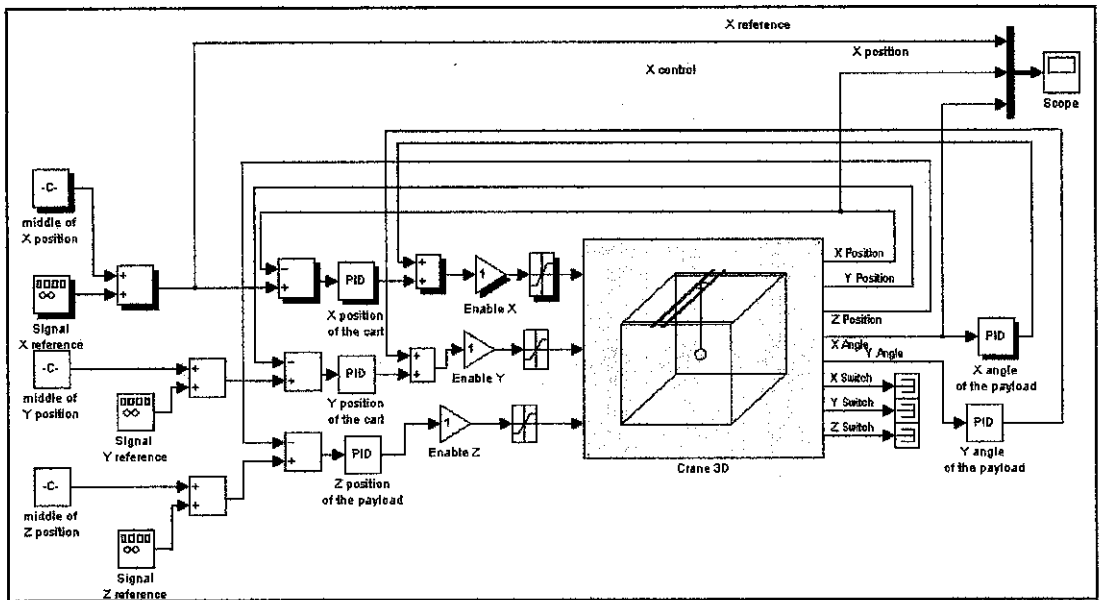


Figure 7 Simulink diagram of the system with PID controller

For full state feedback (FSF) controller, the experiment is conducted using Simulink. Figure 3.4 shows the Simulink diagram of the system with FSF controller. Before the experiment is conducted, the desired pole placement and the controller gain K have to be determined (Refer to Appendix B).

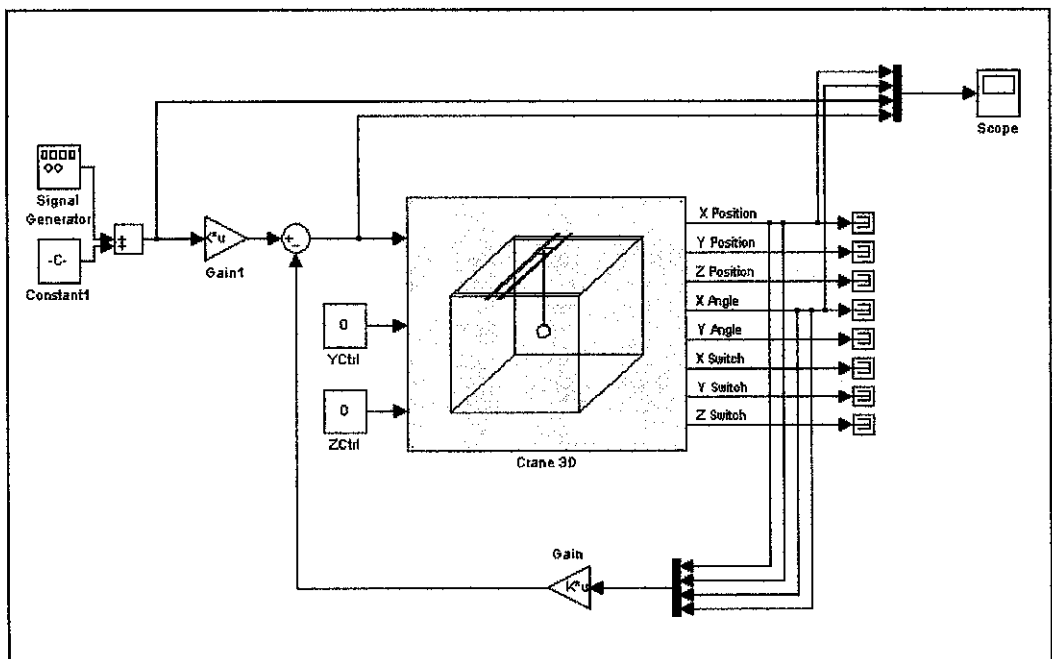


Figure 8 Simulink diagram of the system with FSF controller

CHAPTER 4

RESULTS & DISCUSSION

4.1 Results

4.1.1 Conceptual Study with Overhead Crane (Open Loop System Response)

To get the open-loop response of the system, a unit step input and impulse input have been applied to the system. Figure 9 shows the impulse response of the system and Figure 10 shows the step response of the system. It is observed that the displacement keeps on increasing. It is also observed that there is no damping in the swing motion of the pendulum. Its natural frequency is observed at 0.6Hz.

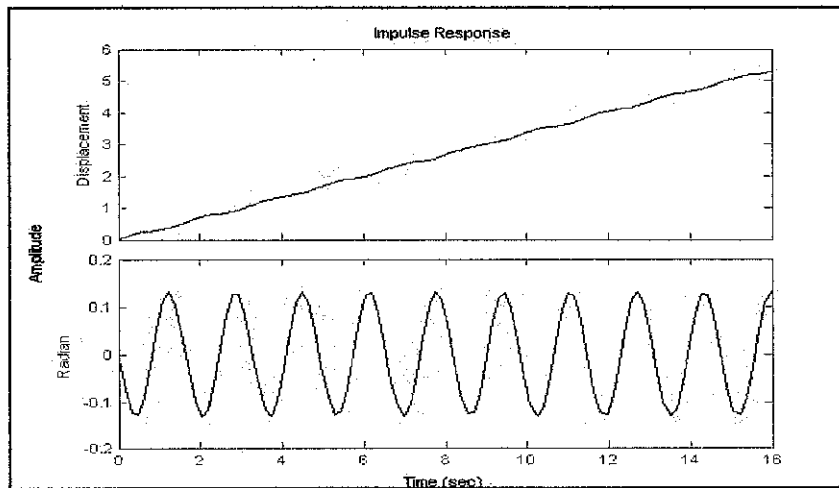


Figure 9 Impulse response of the system

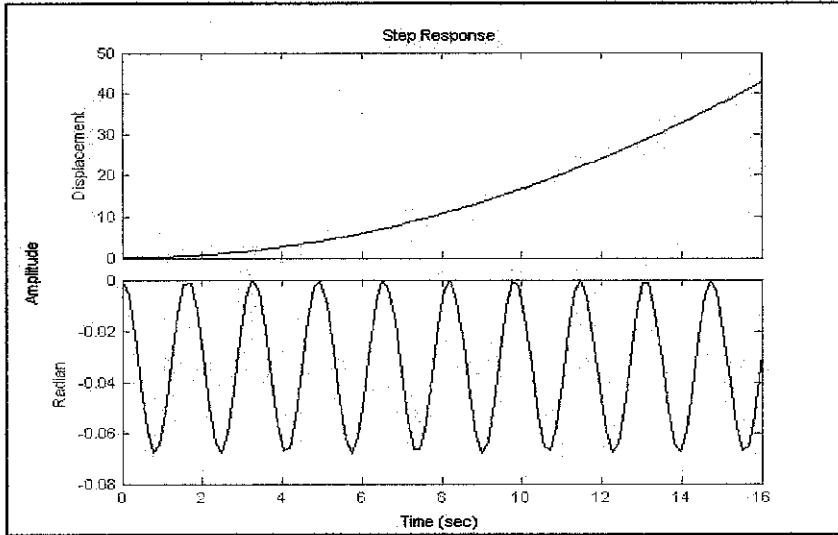


Figure 10 Step response of the system

4.1.2 Mathematical Modelling of the cart and swing dynamic and DC motor

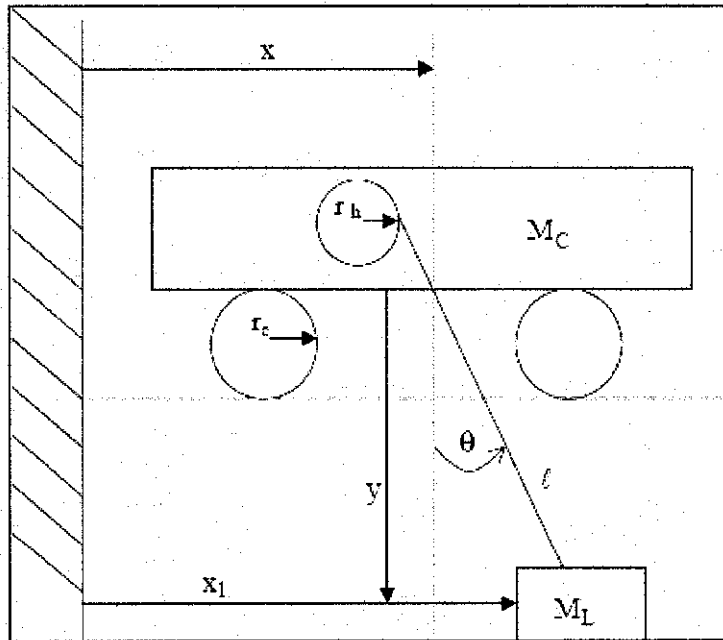


Figure 11 Diagram of the crane³.

³ Figure from G, Costa, *Robust Controller of Gantry Crane*, 1999.

Before the mathematical model is developed, the necessary variables are defined. The model is derived based on [11].

X = horizontal position of cart (m)

M_c = mass of cart and moving rail (kg)

Y = vertical position of load (m)

θ = load angle (rad)

r_c = effective radius of cart (m)

J_c = moment of inertia of cart (kgm^2)

x_l = horizontal position of load (m)

M_L = mass of load

l = length of rope (m)

r_h = effective radius of hoist (m)

J_h = moment of inertia of hoist (kgm^2)

Kinetic energy of cart

$$T_1 = \frac{1}{2} M_c \dot{x}^2 \quad (4.1.1)$$

Kinetic energy of Load (Weight)

$$T_2 = \frac{1}{2} M_L (\dot{x}_l^2 + \dot{y}^2) \quad (4.1.2)$$

Where

$$x_l = x + l \sin \theta \quad y = l \cos \theta \quad (4.1.3)$$

$$\dot{x}_l = \dot{x} + (l\dot{\theta}) \cos \theta \quad \dot{y} = -(l\dot{\theta}) \sin \theta \quad (4.1.4)$$

Moment of Inertia of Cart

$$T_3 = \frac{1}{2} J_c \frac{\dot{x}^2}{r_c^2} \quad (4.1.5)$$

where $x_1 = r_c \theta$

Total Kinetic Energy

$$T = \frac{1}{2} M_c \dot{x}^2 + \frac{1}{2} M_L \left[(\dot{x} + l\dot{\theta} \cos \theta)^2 + (-l\dot{\theta} \sin \theta)^2 \right] + \frac{1}{2} J_c \frac{\dot{x}^2}{r_c^2} \quad (4.1.6)$$

$$T = \frac{1}{2} M_c \dot{x}^2 + \frac{1}{2} M_L \left[\dot{x}^2 + 2\dot{x}l\dot{\theta} \cos \theta + (l\dot{\theta})^2 \cos^2 \theta + (l\dot{\theta})^2 \sin^2 \theta \right] + \frac{1}{2} J_c \frac{\dot{x}^2}{r_c^2} \quad (4.1.7)$$

Total Potential Energy

$$U = -M_L g y = -M_L g l \cos \theta \quad (4.1.8)$$

Lagrangian Equation

Now that all the energy components within the system have been accounted for, the Lagrangian of the system is found by combining (4.1.7) and (4.1.8)

$$L = \frac{1}{2} M_c \dot{x}^2 + \frac{1}{2} M_L \left[\dot{x}^2 + 2\dot{x}l\dot{\theta} \cos \theta + (l\dot{\theta})^2 \cos^2 \theta + (l\dot{\theta})^2 \sin^2 \theta \right] + \frac{1}{2} J_c \frac{\dot{x}^2}{r_c^2} + M_L g l \cos \theta \quad (4.1.9)$$

There is only one external force that is acting on the cart and swing dynamics and that is the force that is applied by the motor to the cart. This force only acts on the co-ordinate of x , which is linear displacement. The θ co-ordinate of the system does not have any external forces that directly act upon it.

Thus

$$\frac{d}{dt} \left[\frac{\partial L}{\partial \dot{x}} \right] - \left[\frac{\partial L}{\partial x} \right] = F \quad (4.1.10)$$

$$\frac{d}{dt} \left[\frac{\partial L}{\partial \dot{\theta}} \right] - \left[\frac{\partial L}{\partial \theta} \right] = 0 \quad (4.1.11)$$

Substituting (4.1.9) into (4.1.10) and evaluating for the 'x' co-ordinate of the system gives

$$\frac{\partial L}{\partial \dot{x}} = M_c \dot{x} + M_L \dot{x} + M_L l \dot{\theta} \cos \theta + J_c \frac{\dot{x}}{r_c^2} \quad (4.1.12)$$

$$\frac{d}{dt} \left[\frac{\partial L}{\partial \dot{x}} \right] = M_c \ddot{x} + M_L \ddot{x} - M_L l \dot{\theta} \dot{\theta} \sin \theta + M_L l \ddot{\theta} \cos \theta + J_c \frac{\ddot{x}}{r_c^2} \quad (4.1.13)$$

$$\frac{\partial L}{\partial x} = 0 \quad (4.1.14)$$

$$F = M_c \ddot{x} + M_L \ddot{x} - M_L l \dot{\theta} \dot{\theta} \sin \theta + M_L l \ddot{\theta} \cos \theta + J_c \frac{\ddot{x}}{r_c^2} \quad (4.1.15)$$

Similarly evaluating for the 'θ' co-ordinate of the system gives

$$\frac{\partial L}{\partial \dot{\theta}} = M_L \dot{x} l \cos \theta + M_L l^2 \dot{\theta} \quad (4.1.16)$$

$$\frac{d}{dt} \left[\frac{\partial L}{\partial \dot{\theta}} \right] = -M_L \dot{x} \dot{\theta} \sin \theta + M_L l \ddot{x} \cos \theta + M_L l^2 \ddot{\theta} \quad (4.1.17)$$

$$\frac{\partial L}{\partial \theta} = -M_L \dot{x} l \dot{\theta} \sin \theta - M_L g l \sin \theta \quad (4.1.18)$$

$$0 = M_L \ddot{x} l \cos \theta + M_L l^2 \ddot{\theta} + M_L g l \cos \theta \quad (4.1.19)$$

Modelling of DC Motor

The DC motors on the system are $\pm 12\text{V}$ armature controlled DC motors. The model of the DC motor described here is based on [12]. The diagram below shows the schematic representation of motor.

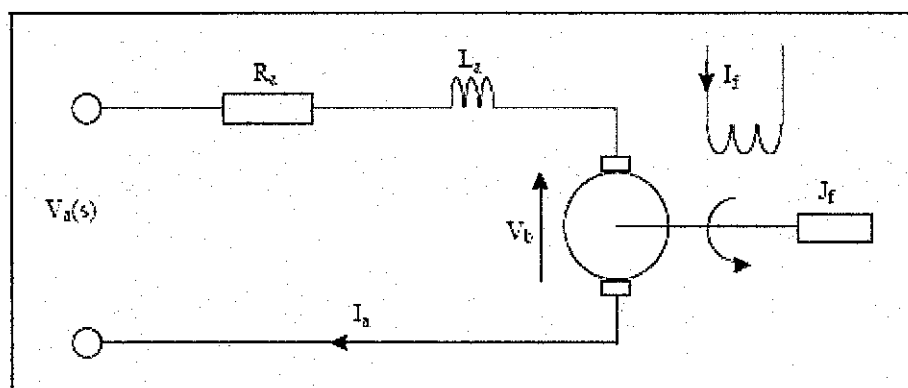


Figure 12 Schematic of an armature controlled DC motor⁴.

⁴ Figure from R.C. Dorf, *Modern Control System 4th Edition*, Addison-Wesley, 1986

R_a = armature resistance

I_a = armature current

$V_a(s)$ = applied armature voltage

Θ = angular position of motor shaft (rad)

J_f = moment of inertia of motor load

f = viscous friction of motor and load

L_a = armature inductance (H)

I_f = field current (A)

V_b = generated back emf (V)

T = developed torque (Nm)

The torque developed is proportional to $I_a(t)$ and the air gap flux Φ

$$T = K_t K_f I_f(t) I_a(t) \quad (4.1.20)$$

where $\phi = K_f I_f(t)$ is a constant.

Since $I_f(t)$ is constant in an armature controller DC motor and K_t , K_f are also constants, then

$$T = K_c I_a(t) \quad (4.1.21)$$

The applied voltage is related to the armature current as follows

$$V_a(t) = R_a I_a(t) + L_a \frac{dI_a(t)}{dt} + V_b(t) \quad (4.1.22)$$

Where $V_b(t)$ is the back emf voltage proportional to the motor's speed. Therefore

$$V_b(t) = K_{emf} \frac{d\Theta}{dt} \quad (4.1.23)$$

Taking the Laplace transform of (4.1.21)-(4.1.23) and substituting (4.1.23) into (4.1.22), the armature current can be represented as

$$I_a(s) = \frac{V_a(s) - K_b \dot{\Theta}(s)}{R_a + L_a s} \quad (4.1.24)$$

Thus substituting (4.1.24) into the Laplace transform of (4.1.21), the torque equation becomes

$$T(s) = K_c \left(\frac{V_a(s) - K_b \dot{\Theta}(s)}{R_a \left(1 + \frac{L_a s}{R_a}\right)} \right) \quad (4.1.25)$$

For many DC motors the time constant $\frac{L_a}{R_a}$ may be neglected as L_a is significantly smaller than R_a . Thus the equation for torque that will be used in the modelling of the system is

$$T = K_c \left(\frac{V_a(s) - K_b \dot{\Theta}(s)}{R_a} \right) \quad (4.1.26)$$

Since it is desired to measure linear position and velocity the following conversion is performed: $\dot{\Theta} = \frac{\dot{x}}{r_c}$ where r_c is the effective radius that converts an angular displacement into its linear equivalent.

$$T = K_c \left(\frac{V_a(s) - K_b \frac{\dot{x}}{r_c}}{R_a} \right) \quad (4.1.27)$$

Torque is described by the following equation $T=FL$ with SI units of (Nm) where L is described as the moment arm, i.e. the perpendicular distance between the line of rotation and the force. Since torque is the force which causes rotation it is used when

one wants to use angular co-ordinates to develop a systems model. In the derivation of the Lagrangian dynamics for the cart system a linear co-ordinate system was chosen, thus (4.1.15) needs to be equated to force (linear co-ordinate) and not torque (angular co-ordinate).

The force equation can be derived by substituting $T=FL$ into (4.1.27). Thus, the force equation of the motor becomes

$$F = K_I \left(\frac{V_a(s) - K_b \frac{\dot{x}}{r_c}}{R_a} \right) \quad (4.1.28)$$

Where $K_I = \frac{K_c}{L}$

From (4.1.28), the motor has been modeled and can be combined with the cart dynamics.

$$K_I \left(\frac{V_a - K_b \frac{\dot{x}}{r_c}}{R_a} \right) = M_c \ddot{x} + M_L \ddot{x} + J_c \frac{\ddot{x}}{r_c^2} \quad (4.1.29)$$

$$M\ddot{x} = u \quad (4.1.30)$$

Where $M = M_c + \frac{J_c}{r_c^2}$

$$M\ddot{x} = \frac{K_I}{R_a} V_a - \frac{K_I K_b}{R_a r_c} \dot{x} \quad (4.1.31)$$

In order to get the transfer function from V_a to x , the equation is transformed using Laplace transform becomes

$$Ms^2 X + \frac{K_I K_b}{R_a r_c} sX = \frac{K_I}{R_a} V_a \quad (4.1.32)$$

$$G(s) = \frac{X(s)}{V(s)} = \frac{\frac{r_c}{K_b}}{M \frac{R_a r_c}{K_I K_b} s^2 + s} = \frac{\frac{r_c}{K_b}}{s(M \frac{R_a r_c}{K_I K_b} s + 1)} \quad (4.1.33)$$

$$u = M\ddot{x} = -\frac{M}{\tau} \dot{x} + \frac{MK}{\tau} V_a \quad (4.1.34)$$

Derivation of pendulum model

Previously, the cart dynamics were modelled and from equation (4.1.34) the system is expanded and also includes the pendulum.

Expressions from the trolley:

$$M\ddot{x} = u - H \quad (4.1.35)$$

$$H = M_L(\ddot{x} + l\ddot{\theta} \cos\theta + l\dot{\theta}^2 \sin\theta) \quad (4.1.36)$$

Expression from the pendulum:

$$M_L(\ddot{x} \cos\theta + l\ddot{\theta}) = -M_L g \sin\theta + H \cos\theta + V \sin\theta \quad (4.1.37)$$

$$J\ddot{\theta} = -Hl \cos\theta - Vl \sin\theta \quad (4.1.38)$$

Combining equation (4.1.36) and (4.1.38)

$$V \sin\theta = -\frac{J}{l} \ddot{\theta} - M_L \ddot{x} \cos\theta - M_L l \ddot{\theta} \cos^2\theta - M_L l \dot{\theta}^2 \sin\theta \cos\theta \quad (4.1.39)$$

Insertion of (4.1.39) into (4.1.38)

$$(J + M_L l^2) \ddot{\theta} = -M_L l \ddot{x} \cos \theta - M_L l g \sin \theta \quad (4.1.40)$$

This equation can be linearised by assuming that $\sin \theta \approx \theta$, $\sin \theta^2 \approx 0$, $\cos \theta \approx 1$ and $\dot{\theta}^2 \approx 0$. This assumption can be made for small θ .

$$(J + M_L l^2) \ddot{\theta} = -M_L l (\ddot{x} + g \theta) \quad (4.1.41)$$

Combining (4.1.35) and (4.1.36):

$$M \ddot{x} = u - M_L x (\ddot{x} + l \ddot{\theta} \cos \theta + l \dot{\theta}^2 \sin \theta) \quad (4.1.42)$$

Linearising (4.1.42) by using the previous assumptions:

$$(M + M_L) \ddot{x} = u - M_L l \ddot{\theta} \quad (4.1.43)$$

From the linearised equations (4.1.41) and (4.1.43) and the knowledge that a mathematical pendulum has $J = M_L l^2$ the final result can be derived:

$$\ddot{x} = \frac{M_L g \theta + 2u}{2M + M_L} \quad (4.1.44)$$

$$\ddot{\theta} = \frac{-g \theta (M + M_L) - u}{L(2M + M_L)} \quad (4.1.45)$$

Total system model state space representation

Now that the motor has been modelled, it can be combined with the cart and swing dynamics to give an overall system transfer function. Thus, combining (4.1.10) and (4.1.15), the state-space representation has the form:

$$\begin{bmatrix} \dot{x}_1 \\ \dot{x}_2 \\ \dot{x}_3 \\ \dot{x}_4 \end{bmatrix} = \begin{bmatrix} 0 & 1 & 0 & 0 \\ 0 & a & b & 0 \\ 0 & 0 & 0 & 1 \\ 0 & c & d & 0 \end{bmatrix} \begin{bmatrix} x_1 \\ x_2 \\ x_3 \\ x_4 \end{bmatrix} + \begin{bmatrix} 0 \\ e \\ 0 \\ f \end{bmatrix} u$$

$$y = \begin{bmatrix} 1 & 0 & 0 & 0 \\ 0 & 0 & 1 & 0 \end{bmatrix} \begin{bmatrix} x_1 \\ x_2 \\ x_3 \\ x_4 \end{bmatrix} + \begin{bmatrix} 0 \\ 0 \end{bmatrix} u$$

The states of the cart and swing dynamics are defined as follows

$x_1 = \text{cart position} = x$

$x_2 = \text{cart velocity} = \dot{x} = \dot{x}_1$

$x_3 = \text{swing angle} = \theta$

$x_4 = \text{swing velocity} = \dot{\theta} = \dot{x}_3$

$u = \text{the applied motor voltage} = V_a$

$$a = \frac{-2M}{\tau(2M + M_L)}$$

$$b = \frac{M_L g}{2M + M_L}$$

$$c = \frac{M}{l\tau(2M + M_L)}$$

$$d = \frac{-g(M + M_L)}{l(2M + M_L)}$$

$$e = \frac{2MK}{\tau(2M + M_L)}$$

$$f = \frac{-MK}{l\tau(2M + M_L)}$$

Hoist Model

Using the Lagrangian dynamics method defined previously, the hoist dynamics of the system can be derived. In the modelling of the hoist dynamics it is assumed the swing angle is zero. Thus, $z = 1$ and the moment of inertia is small and negligible.

Kinetic energy of Hoist

$$T_1 = \frac{1}{2} M_L \dot{z}^2 \tag{4.1.46}$$

Potential energy of Hoist

$$U = -M_L g z \tag{4.1.47}$$

The Lagrangian for the system is found by combining (4.1.46) and (4.1.47)

$$L = \frac{1}{2} M_L \dot{z}^2 - M_L g z \tag{4.1.48}$$

From the definition of the Lagrangian dynamics it is known that

$$\frac{d}{dt} \left[\frac{\partial L}{\partial \dot{z}} \right] - \left[\frac{\partial L}{\partial z} \right] = F \quad (4.1.49)$$

$$\frac{d}{dt} \left[\frac{\partial L}{\partial \dot{z}} \right] = M_L \ddot{z} \quad (4.1.50)$$

$$F = M_L \ddot{z} - M_L g \quad (4.1.51)$$

We know that the force equation for a motor is

$$F = K_I \left(\frac{V_a(s) - K_b \frac{\dot{z}}{r_H}}{R_a} \right) \quad (4.1.52)$$

Combining (4.1.51) and (4.1.52) the equation for the hoist dynamic is

$$K_I \left(\frac{V_a(s) - K_b \frac{\dot{z}}{r_c}}{R_a} \right) = M_L \ddot{z} - M_L g \quad (4.1.53)$$

$$F = K_I \left(\frac{V_a(s) - K_b \frac{\dot{z}}{r_c}}{R_a} \right) \quad (4.1.54)$$

From previous section, the equation can be simplified as follows:

$$M_L \ddot{z} = \frac{K_I}{R_a} V_a - \frac{K_I K_b}{R_a r_H} \dot{z} - M_L g \quad (4.1.55)$$

$$\ddot{z} = -\frac{2}{\tau M_L} \dot{z} + \frac{2K}{\tau M_L} V_a + g \quad (4.1.56)$$

The state of the hoisting system are defined as follows

$$x_5 = \text{rope length} = z$$

$$x_6 = \text{rope velocity} = \dot{z} = \dot{x}_5$$

$$u = \text{the applied motor voltage} = V_a$$

Linearisation techniques are another method of removing constant terms (like gravitational forces) from a model. This will cause any constant terms to go to zero when the partial differential is taken of the system equations about the operating point. This explains the final state space representation without the gravitational forces. The state space representation of the hoist model is now given as

$$\begin{bmatrix} \dot{x}_5 \\ \dot{x}_6 \end{bmatrix} = \begin{bmatrix} 0 & 1 \\ 0 & h \end{bmatrix} \begin{bmatrix} x_5 \\ x_6 \end{bmatrix} + \begin{bmatrix} 0 \\ i \end{bmatrix} u$$

$$y = \begin{bmatrix} 1 & 0 \end{bmatrix} \begin{bmatrix} x_5 \\ x_6 \end{bmatrix}$$

Where

$$h = \frac{-2}{\tau M_L}$$

$$i = \frac{2K}{\tau M_L}$$

4.1.3 Model Verification

The linearised model of the system was derived. After linearisation, the parameter measurements and calculations are determined. The masses of the cart (M) and load (M_L) were measured whilst all the other parameters needed were determined by experiments.

The physical transfer function from input voltage to the horizontal position derived has the form

$$G(s) = \frac{X(s)}{V(s)} = \frac{\frac{r_c}{K_b}}{s(M \frac{R_a r_c}{K_j K_b} s + 1)} \quad (4.1.46)$$

Many of the variables in the physical model are hard to determine, such as torque and different resistances. This is because every motor has its own characteristics. Thus, instead of determining all the unknown parameters in equation (4.1.46), all the unknown parameters can be determined by simplifying equation (4.1.46) to equation (4.1.47) as shown below.

$$G(s) = \frac{K}{s(\tau s + 1)} \quad (4.1.47)$$

Only two parameters need to be determined. The parameters are determined experimentally. A step input is given to the model and the values of K and τ are determined by fitting the step response of the equation (4.1.47) to the measured step response as shown in Figure 13.

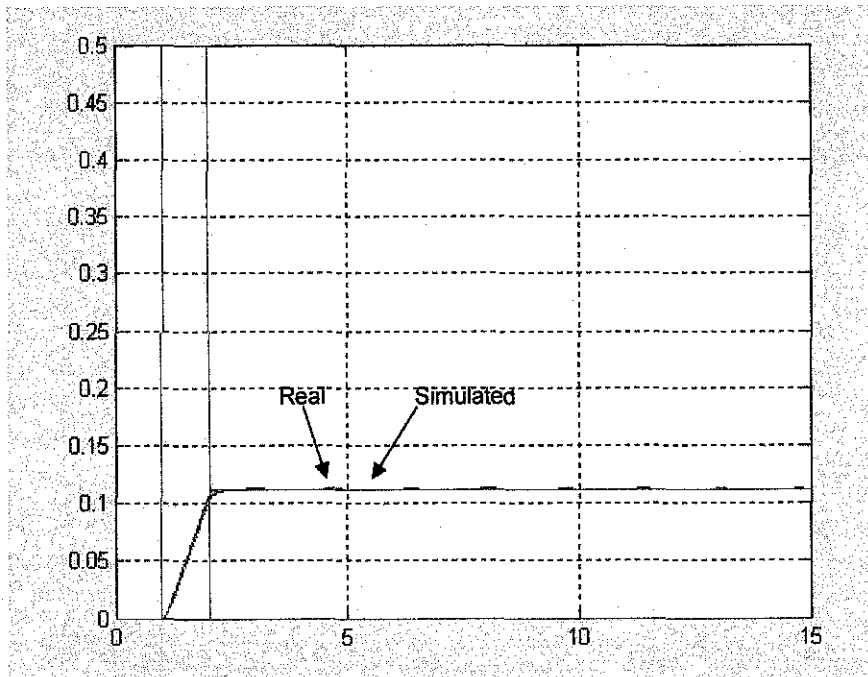


Figure 13 Real and simulated position of x

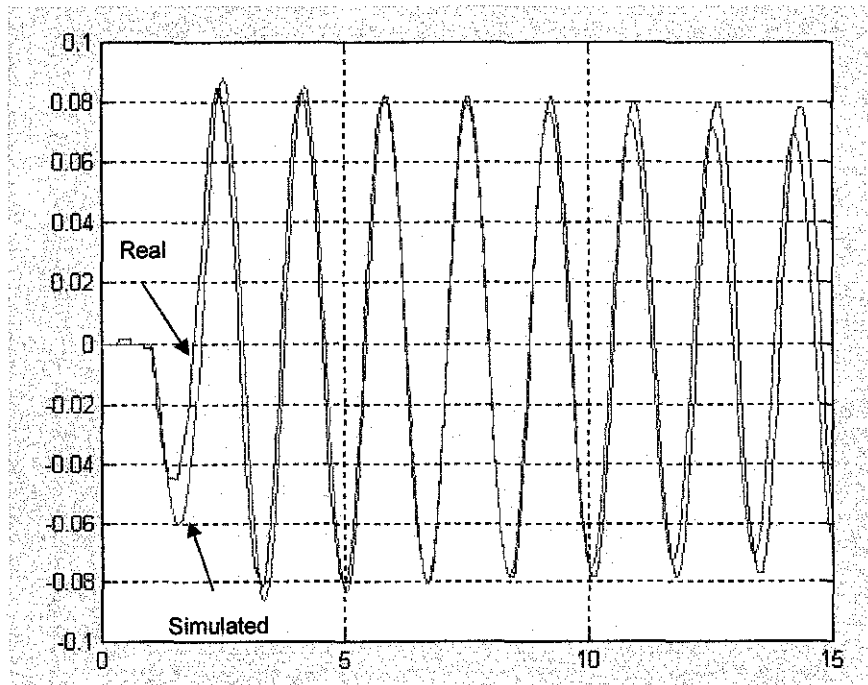


Figure 14 Real and simulated angle of x

Table 3 Values of the parameters (x-direction)

Parameter	Value	Description
M	7 kg	Mass of cart and moving rail
M_L	0.5 kg	Mass of load
τ	0.09	Time constant for cart
K	0.225	Gain of cart
K_{vp}	0.025	Gain of angle sensor
l	0.25 m	Length of cable

$$\begin{bmatrix} \dot{x}_1 \\ \dot{x}_2 \\ \dot{x}_3 \\ \dot{x}_4 \end{bmatrix} = \begin{bmatrix} 0 & 1 & 0 & 0 \\ 0 & -10.728 & 0.3383 & 0 \\ 0 & 0 & 0 & 1 \\ 0 & 21.46 & -20.32 & 0 \end{bmatrix} \begin{bmatrix} x_1 \\ x_2 \\ x_3 \\ x_4 \end{bmatrix} + \begin{bmatrix} 0 \\ 2.4138 \\ 0 \\ -5.36 \end{bmatrix} u$$

$$y = \begin{bmatrix} 1 & 0 & 0 & 0 \\ 0 & 0 & 1 & 0 \end{bmatrix} \begin{bmatrix} x_1 \\ x_2 \\ x_3 \\ x_4 \end{bmatrix} + \begin{bmatrix} 0 \\ 0 \end{bmatrix} u$$

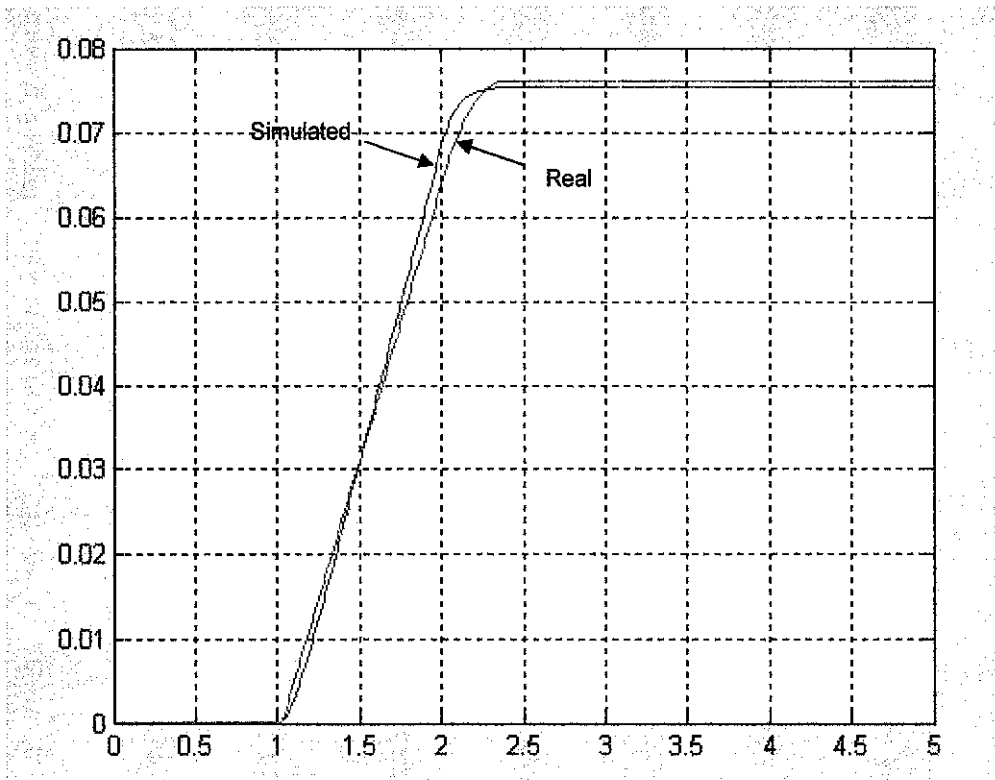


Figure 15 Real and simulated position of z

Table 4 Values of the parameters (z-direction)

Parameter	Value	Description
M_L	0.5 kg	Mass of load
τ	0.09	Time constant for cart
K	0.15	Gain
l	0.35 m	Length of cable

$$\begin{bmatrix} \dot{x}_5 \\ \dot{x}_6 \end{bmatrix} = \begin{bmatrix} 0 & 1 \\ 0 & -44.44 \end{bmatrix} \begin{bmatrix} x_5 \\ x_6 \end{bmatrix} + \begin{bmatrix} 0 \\ 6.67 \end{bmatrix} u$$

$$y = \begin{bmatrix} 1 & 0 \end{bmatrix} \begin{bmatrix} x_5 \\ x_6 \end{bmatrix}$$

4.1.4 PD Controller

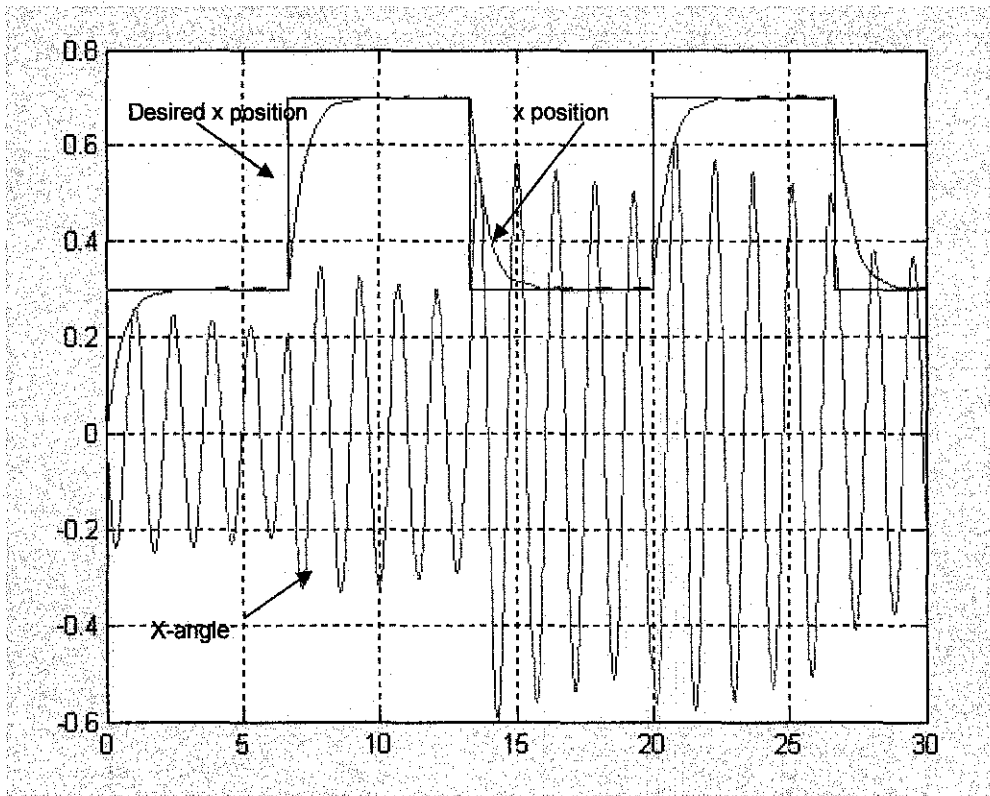


Figure 16 x position, x-reference, x-angle with PD controller without the angle swing feedback

Figure 16 shows the output response from the system with PD controller without the angle swing feedback. It can be observed that the PD controller only controls the position of the cart and has no control over the swing motion of the pendulum. The x angle keeps on increasing and there is no sign of damping.

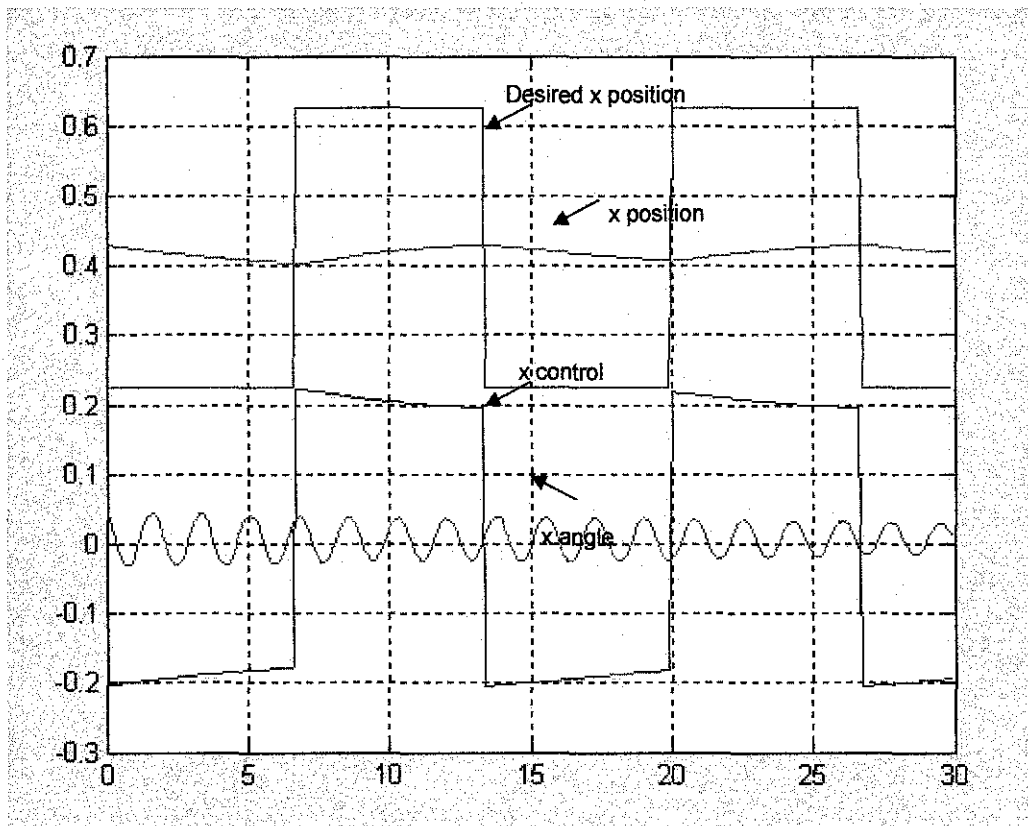


Figure 17 Control, x position, x-reference, x-angle without controller

Figure 17 shows the control, x-position, x-reference and x-angle without controller. It is shown that the x-position does not reach the desired x-position at all. The static error of x-position is large. Other than that, the swing frequency remains constant and there is no sign of damping in the swing. Without the controller, the objective of this project which is to reduce the swing of the load and ensure accurate cart position could not be achieved.

On the other hand, Figure 18 shows the control, x-position, x-reference and x-angle with P controller. It is observed that there is improvement in the cart positioning. The x-position reaches the desired x-position although there is some delay. Thus the static error of x-position is reduced. Whenever the direction changed, the x-angle has some overshoot. However, the x-angle dampens which is better than having constant swing frequency.

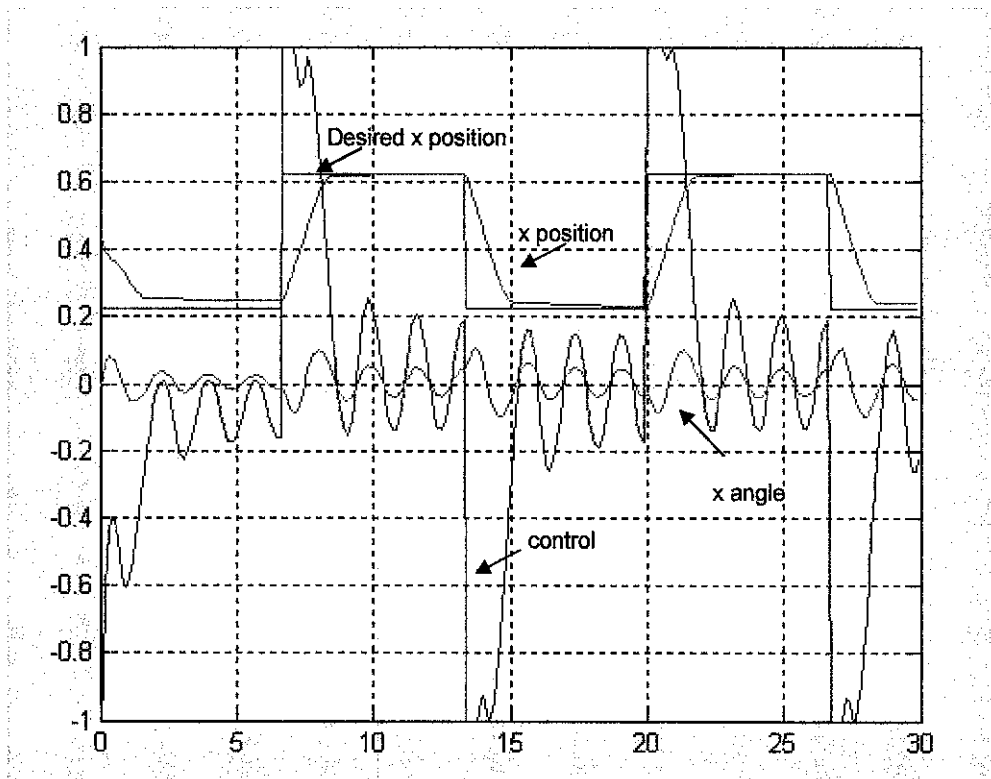


Figure 18 Control, x position, x-reference, x-angle with P controller

In figure 19, it can be seen that the control is saturated. This is the result of the high gain P. The control will be more saturated if the higher gain P is imposed to the system. The same outcome is also obtained if two controllers are active (see Figure 19). This is because one control signal serves for two purposes such as following the desired value of the cart x position and simultaneously stabilizing the load in its hanging down position. If the gain P is too high, the x-position has an overshoot before it reaches the desired value (see Figure 20). The overshoot in the x-angle also increases and it takes a longer time to stabilize the load.

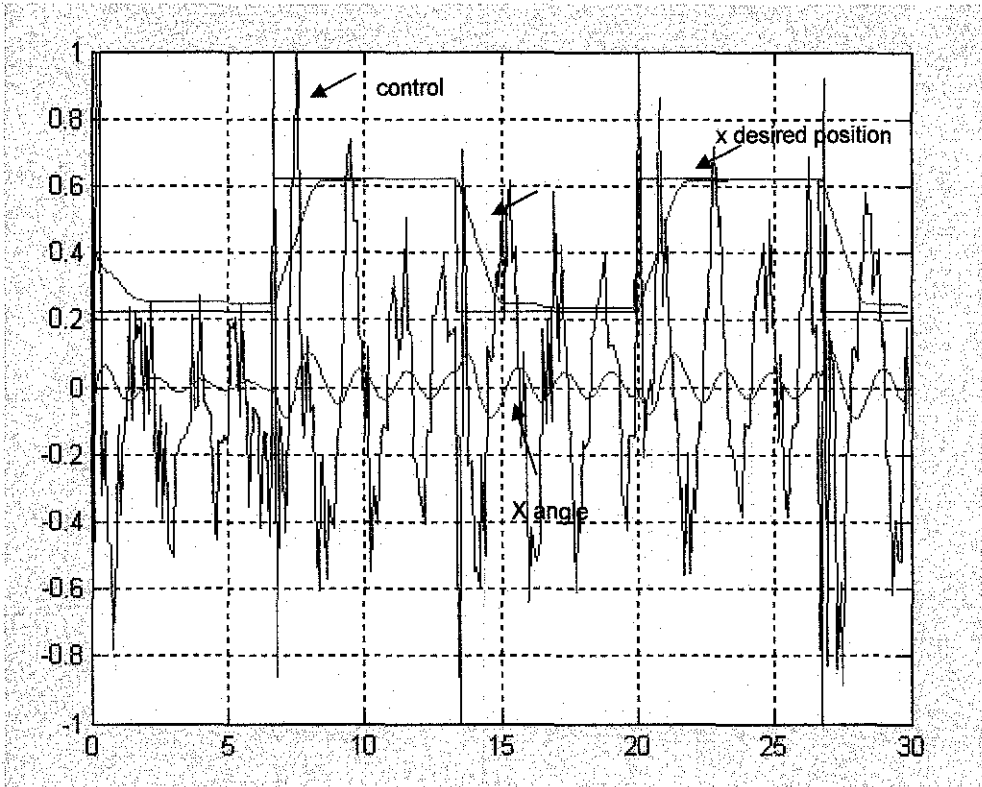


Figure 19 x-control, x position, x-reference, x-angle with PD controller

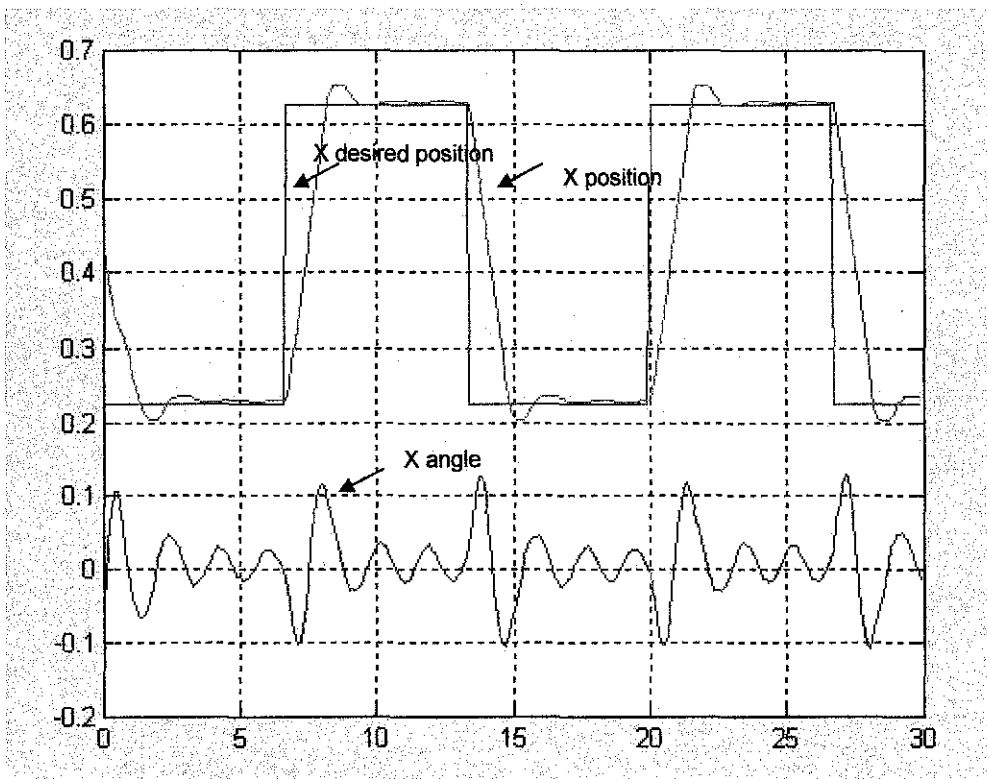


Figure 20 x position, x-reference, x-angle with $K_p = 10$

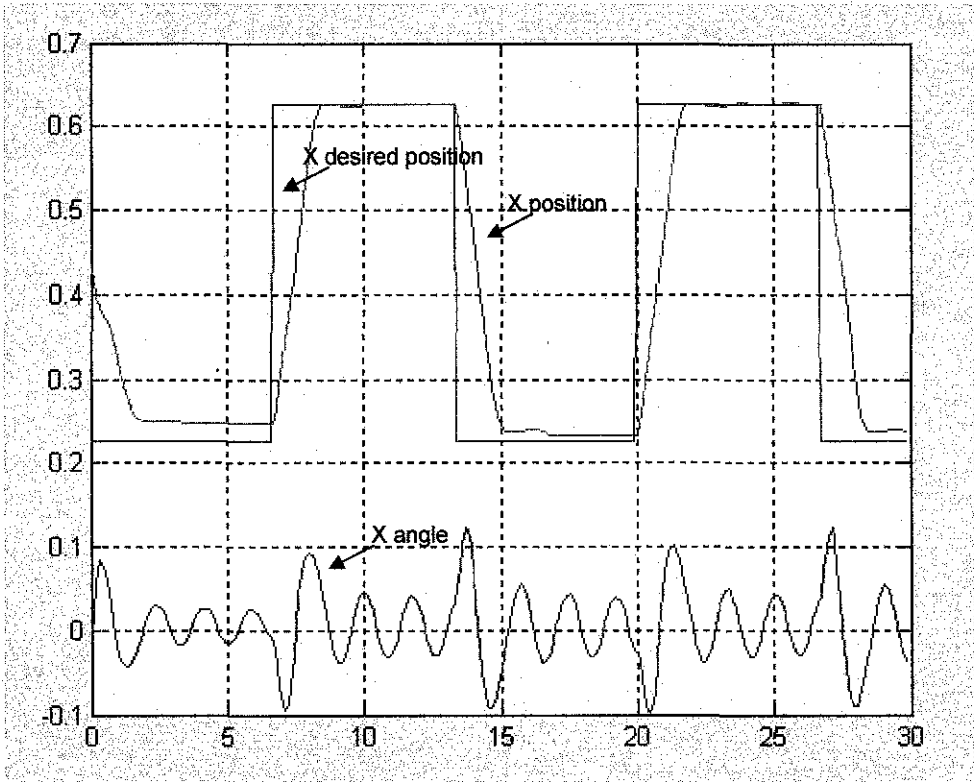


Figure 21 x position, x-reference, x-angle with $K_{p1} = K_{p2} = K_{d1} = K_{d2} = 5$

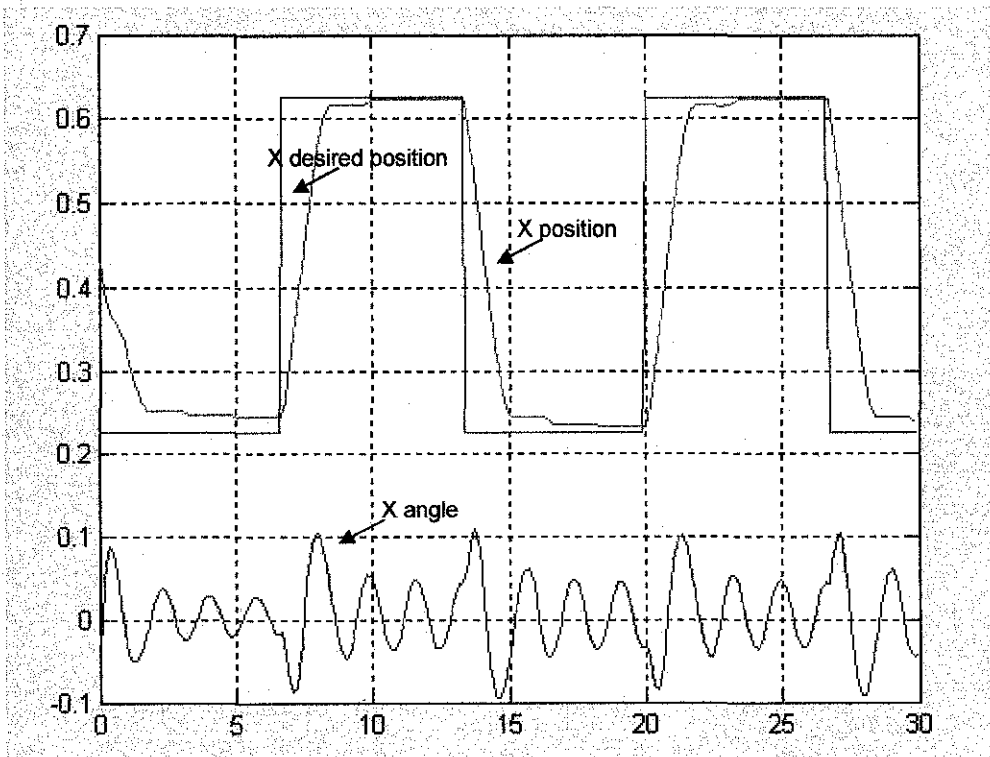


Figure 22 x position, x-reference, x-angle with $K_{p1} = 5, K_{d1} = 4, K_{p2} = 4, K_{d2} = 2$

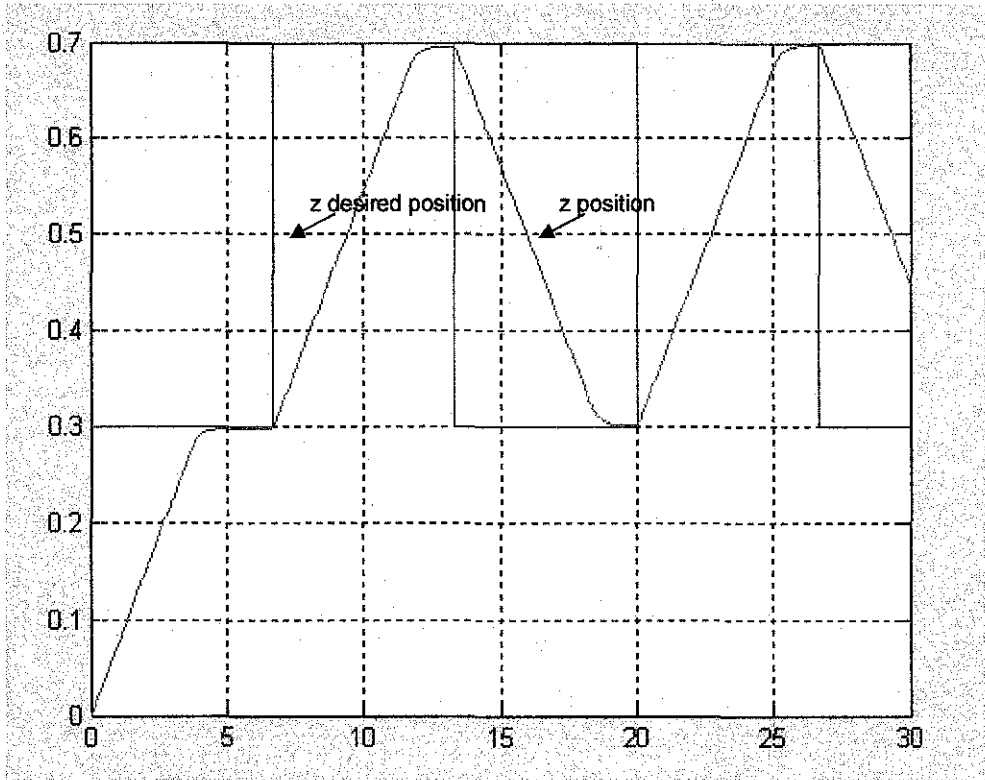


Figure 23 z-position and z-reference with $K_p = 10$ and $K_d = 5$

All the suitable K_p and K_d for x-direction and z-direction have been summarized in the table below.

Table 5 PD constant values for x-direction and z-direction

	PD constant	Value
X-Direction	K_{p1}	5
	K_{d1}	4
	K_{p2}	4
	K_{d2}	2
Z-Direction	K_p	10
	K_d	5

4.1.5 Full State Feedback Using Pole Placement Method (FSF)

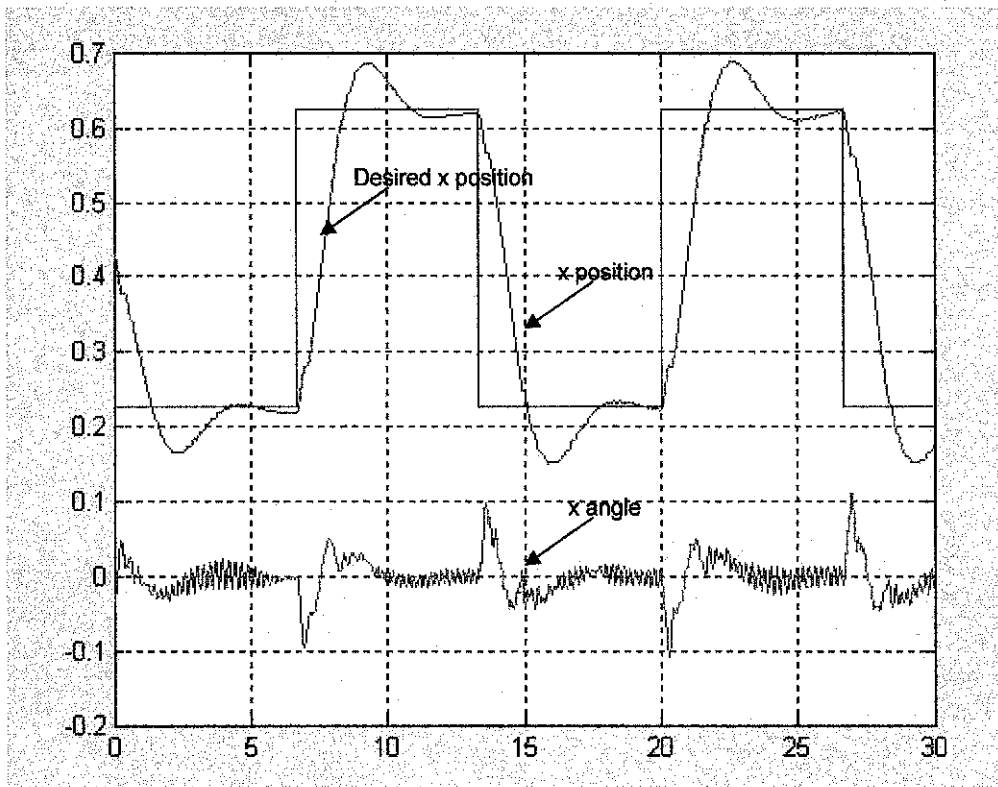


Figure 24 x position, x-reference, x-angle with FSF controller

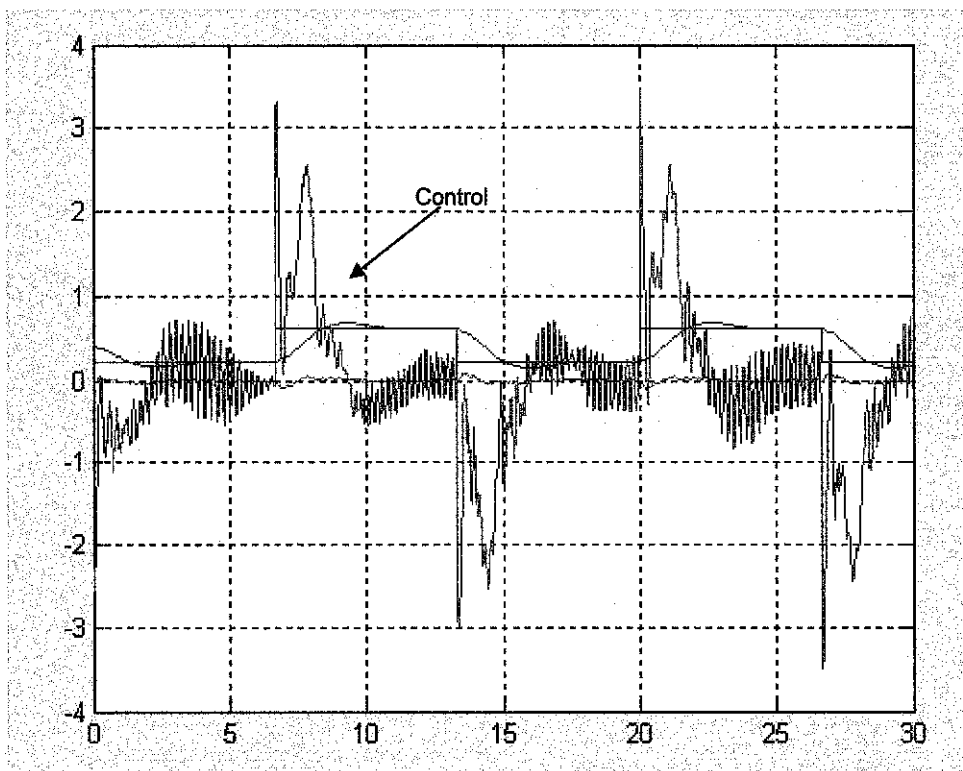


Figure 25 x-control, x position, x-reference with FSF controller

Figure 24 shows the x-position, x-reference and x-angle with full-state feedback controller. It can be seen that the x-position reaches the desired location but with an overshoot. As for the x-angle, it is shown that the angle is very small. This shows that the swinging of the payload is damping. Compared to the x-angle from Figure 22, this angle is smaller. In figure 25 it is shown that the control is saturated.

4.2 Discussion

4.2.1 Conceptual Study with Overhead Crane (System Description)

To obtain the mathematical model, it is assumed that the pendulum can oscillate only in the plane of the paper. With this constraint, only one coordinate- the angular displacement of the rod, θ (rad) – is required for a complete specification of the pendulum's geometric location. Such a mechanical system is said to have one degree of freedom. A further assumption is that the only force acting on the system is gravitational.

The free-body diagram in Figure 1 shows the rotational mechanical system displaced by an angle θ from its equilibrium position. The negative sign indicates that the direction or the moment is in the opposite direction to θ . The dynamic model of the system has been derived using Newtonian mechanics. The system dynamics are shown in Equation (4.2.1) and (4.2.2). ([13] Page 782-784)

$$(M + m)\ddot{x} + ml\ddot{\theta} \cos\theta - ml\dot{\theta}^2 \sin\theta = F \quad (4.2.1)$$

$$ml^2\ddot{\theta} + ml\ddot{x} \cos\theta + mgl \sin\theta = 0 \quad (4.2.2)$$

M = mass of the cart in Kg

m = mass of payload at the end of the pendulum in Kg

\ddot{x} = acceleration of the car

θ = swing angle

$\dot{\theta}$ = velocity of the swing angle

$\ddot{\theta}$ = acceleration of the swing angle

F = the applied force in Newton

g = acceleration due to gravity

l = length of pendulum

The equations are nonlinear because of the sinusoidal term, but it may be linearized by assuming that only small perturbations (swings) will occur about the operating point.

With an assumption that the swing angle remains small so that $\sin\theta \approx \theta$ and $\cos\theta \approx 1$, the system equations may be linearized as follows:

$$(M + m)\ddot{x} + ml\ddot{\theta} = F \quad (4.2.3)$$

$$l\ddot{\theta} + \ddot{x} + g\theta = 0 \quad (4.2.4)$$

To represent the Equations (4.2.3) and (4.2.4) in a state space form, four states have been chosen as follows:

$$x_1 = x$$

$$x_2 = \dot{x}$$

$$x_3 = \theta$$

$$x_4 = \dot{\theta}$$

Representing them in a matrix form, $\dot{X} = AX + BU$ and $Y = CX + DU$, where A is the system dynamics matrix, U is the input, Y is the output, B , C and D are coefficient matrix.

The matrix, A , B , C and D are as follows:

$$\begin{bmatrix} \dot{x}_1 \\ \dot{x}_2 \\ \dot{x}_3 \\ \dot{x}_4 \end{bmatrix} = \begin{bmatrix} 0 & 1 & 0 & 0 \\ 0 & 0 & mg/M & 0 \\ 0 & 0 & 0 & 1 \\ 0 & 0 & -g(M+m)/Ml & 0 \end{bmatrix} \begin{bmatrix} x_1 \\ x_2 \\ x_3 \\ x_4 \end{bmatrix} + \begin{bmatrix} 0 \\ 1/M \\ 0 \\ -1/Ml \end{bmatrix} [F] \quad (4.2.5)$$

And the output equations are as follows:

$$\begin{bmatrix} x \\ \theta \end{bmatrix} = \begin{bmatrix} 1 & 0 & 0 & 0 \\ 0 & 0 & 1 & 0 \end{bmatrix} \begin{bmatrix} x_1 \\ x_2 \\ x_3 \\ x_4 \end{bmatrix} + \begin{bmatrix} 0 \\ 0 \end{bmatrix} [F] \quad (4.2.6)$$

For simulation purposes, the parameters are assigned as follows:

$M = 2\text{kg}$, $m = 1\text{kg}$, $l = 1\text{m}$, to get the A , B and C matrixes in numerical values.

The A , B and C matrix are given as

$$A = \begin{bmatrix} 0 & 1 & 0 & 0 \\ 0 & 0 & 4.9 & 0 \\ 0 & 0 & 0 & 1 \\ 0 & 0 & -14.7 & 0 \end{bmatrix}, \quad B = \begin{bmatrix} 0 \\ 0.5 \\ 0 \\ -0.5 \end{bmatrix}, \quad C = \begin{bmatrix} 1 & 0 & 0 & 0 \\ 0 & 0 & 1 & 0 \end{bmatrix}$$

The D matrix is a zero matrix; it physically represents the part of input, which produces the output, bypassing the system dynamics.

The system described by Equation (4.2.5) and Equation (4.2.6) has only one control input, but has two states, x and θ to be controlled.

From Figure 9 and Figure 10, it is observed that the displacement keeps on increasing. It is because there is no friction in the simulated system. It is also observed that there is no damping in the swing motion of the pendulum. The amplitude of the swing motion is constant throughout the time. Its natural frequency is observed at 0.6Hz. One cycle of the swing takes 1.67s. From the simulated system, it is shown that the

system is marginally stable. The roots are 0, 0, 0+3.8341i and 0-3.8341i. All the roots are in the left half-plane and have its two roots on the $j\omega$ -axis.

4.2.2 Mathematical Modelling of the cart and swing dynamic and DC motor

The model of the system is derived using Lagrangian dynamics and electromechanical modelling techniques. Lagrangian equation provides a means of determining the equation of motion for conservative and non-conservative systems. Since it is assumed that the system has no energy losses, a conservative approach in the derivation of the Lagrangian equations can be used. The mathematical equation for determining the dynamics of a system using Lagrangian equations is given as:

$$\frac{d}{dt} \left[\frac{\partial L}{\partial \dot{q}_i} \right] - \left[\frac{\partial L}{\partial q_i} \right] = F_i \quad \text{for } i = 1, 2, \dots, n$$

Where i = number of degrees of freedom

F_i = net external forces acting in the direction q

q_i = set of generalized co-ordinates, where $i = 1, 2, 3, \dots, n$

L = system Lagrangian which is comprised of the kinetic and potential energy

The Lagrangian for the system is given as:

$$L = T - U$$

Where T = Total Kinetic energy of the system

U = Total Potential Energy of the system

The main disadvantage with the basic model is that it does not take various frictions into account. There are several different frictions that will be taken into account in the modified model. The friction force on the pendulum, which has both a coulomb and a viscous term, can be described with the equation below:

$$F_{fp} = K_v \dot{\phi} + K_c \operatorname{sgn}(\dot{\phi}) \quad (4.2.7)$$

By adding the friction equation for the pendulum motion the model is modified. The equation that describes the pendulum forces is presented in a general form below:

$$J\ddot{\phi} = -C_1 \dot{\phi} - C_2 \phi - K_v \dot{\phi} - K_c \operatorname{sgn}(\dot{\phi}) \quad (4.2.8)$$

As described in equation (4.2.7) the friction force will damp the oscillating motion of the pendulum. Instead of using the mass, the torque J is used in the equation. The friction is not dependent of the mass but of the torque in the rotation sensor. The last two terms are the friction terms, which are dependent of the angular velocity. The choice of angle sensor, which has very low friction, and the relatively long beam between the sensor and the cable, makes it possible to assume that the coulomb friction is very small. The equation can therefore be simplified to:

$$F_{fp} = K_{vp} \dot{\phi} \quad (4.2.9)$$

The constant K_{vp} was determined by increasing the value until the amplitude of the simulated curve had the same amplitude as the real measurements. This force is added to the force equation of the pendulum. From Figure 14, it is shown that the simulated amplitude is similar to the real amplitude.

4.2.3 PD Controller

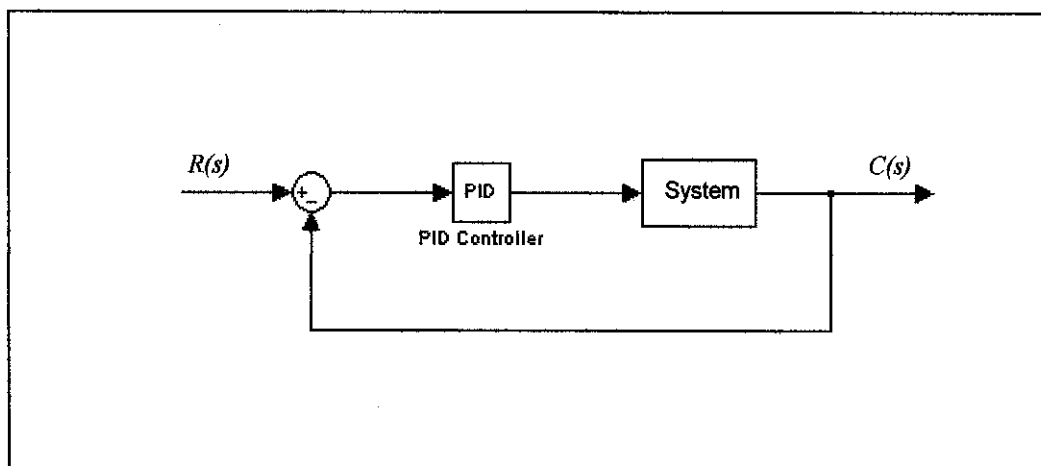


Figure 26 A block diagram of a system with PID controller

The objective of the crane controller is to move the cart to a given location and stop the swing as quickly as possible. In order to find the good values for the gains it is necessary to examine the behaviours of the crane for different gains values. In the experiments, the behaviours of the crane for low, medium and high gains values have been examined.

The values of Critical Gain, K_{cr} and Critical Period, P_{cr} are set to be 13.35 and 4.3 respectively. Thus the values of K_p is 8.01 and P_d is 0.54. From Figure 6, it can be observed that only the cart position, x , has been used for the feedback loop. The PD controller only controls the position of the cart and has no control over the swing motion of the pendulum. This can be seen in Figure 16. Since this control loop does not reduce the swing motion of the pendulum, a controller with swing angle feedback is designed. The diagram of the control system is shown in Figure 7.

In general it can be said that the faster the motor runs the higher the overshoot will be when the target value is reached. Furthermore, the faster the motor is running a quicker response is seen. In the experiment, it is shown that with high gain K_{pl} the cart position reaches the desired position. However, if the gain K_{pl} is very high, the cart response will have an overshoot. By making the gain K_{pl} higher does not make the cart reaches the desired position faster. The x-angle controller is improved by

extending it from a P controller to a PD controller. After the proportional gain K_{p2} has been determined, the derivative gain K_{d2} is increased to dampen the overshoot. The high gains K_{d1} and K_{d2} result in the saturation of the control.

4.2.4 Full State Feedback (FSF) using Pole Placement Method

In this section, the design of the full state feedback controller using the pole placement method will be presented. It is observed that the open-loop crane system is marginally stable. It is also observed that the open-loop crane system is fully controllable.

The desired pole locations are chosen using the ITAE method. The dominant 2nd order poles are determined by using the 2nd order polynomial. The polynomial has been given in equation (4.2.10)

$$s^2 + 1.4\omega_n s + \omega_n^2 \quad (4.2.10)$$

For the third and fourth desired poles, are selected 10 times higher than the real part of the real part of the dominant 2nd order poles and at the left-hand plane. Thus, the desired pole locations are given as follows:

$$\text{Poles} = [-15.0000 \quad -10.0000 \quad -1.1200 + 1.1426i \quad -1.1200 - 1.1426i]$$

The value, ω_n has been determined as 1.6 to satisfy the desired control objectives as stated below:

- Settling time < 8 sec
- % Overshoot < 10%

Using MATLAB (Appendix B), the full state feedback gain matrix has been calculated as follows:

$$K = [8.1295 \quad 0.5720 \quad -28.4553 \quad -2.8230]$$

Full state feedback process is quite simple as it can be automated in MATLAB using `acker` and/or `place` command especially for MIMO system. Any arbitrary desired pole location can be selected by proper design. In root locus, only one parameter can be designed which restricts the poles to lie only on the locus. The poles are selected using ITAE method which is alternate pole shaping method. However, the problem using this method is that it completely ignored the control effort required.

CHAPTER 5

CONCLUSION & RECOMMENDATION

Cranes are popularly used in industry to carry heavy loads. It is found that the swing in the suspended load limits the operational efficiency. The mathematical model of the cart and swing dynamics has been derived from the Lagrangian dynamics and electromechanical theory. Besides that, the model verification was done to determine whether the derived model is sufficient enough to represent the real-time system. From the observation made of the real-time system and the justification presented in section 4, it is concluded that the mathematical derived model is loosely coupled and close enough to the real-time system. The PD-controller and FSF using pole placement method have been designed as the anti-swing controller for this project. From the results, it is proven that the controllers manage to control the cart position and reduce the swing angle. Conclusively, the objectives for this project are achieved.

For future work, it is recommended that the y-direction to be included in the controller design. Experiments with advanced controllers should be considered. A robust controller can be designed using the H^∞ method. This controller can then be used to handle different payloads and lengths of the lift-line.

All the motor constants used in this project were all estimated. Thus, experiments should be conducted to obtain the motor constants to ensure higher accuracy. Besides that, the encoder which was used to measure the swing motion of the load should be included in the derivation of the model.

REFERENCES

- [1] Yoon, J.S., et al, *Various Control Schemes for Implementation of the Anti-Swing Crane*. In ANS 6th Topical Meeting on Robotics and Remote Systems. 1994.

- [2] Noakes, M. W., R.L. Kress, and G.T. Appleton. *Implementation of Damped Oscillation Crane Control for Existing AC Induction Motor-Driven Cranes*. In ANS 5th Topical Meeting on Robotics and Remote Systems. 1993.

- [3] Parker, G.G., et al. *Experiment verification of a Command Shaping Boom Crane Control System*. In American Control Conference. 1999. San Diego, CA.

- [4] S.Nise, Norman, *Control Systems Engineering*. United States: Wiley International Edition, 2004

- [5] Noriaki Miyata and Tetsuji Ukite, *Development of Feedforward Anti-Sway Control for Highly Efficient and Safety Crane Operatio*. Mitsubishi Heavy Industries, Ltd, Technical Review Vol.38 No.2. Jun 2001.

- [6] Lee, H.H., *Modeling and Control of a Three-Dimensional Overhead Crane*. Journal of Dynamic Systems, Measurement and Control. 1998.

- [7] John T. Wen, Dan O.Popa, Gustavo Montemiyor and Perter L. Liu, *Human Assisted Impedance Control of Overhead Crane*.

- [8] Ji Sup Yoon, Byng Suk, *Various Control Schemes for Implementation of the Anti-swing Crane*. Korea Atomic Energy Research Institute.

- [9] MarekRychlik, "Lagrangian mechanics", 9 February 1997,
<http://alamos.math.arizona.edu/~rychlik/556-dir/mechanics/>

- [10] Jan Jantzen, *Tuning Of Fuzzy PID Controllers*, Tech. Report no 98-H 871 (fpid), April 16, 1999, Technical University of Denmark, Department of Automation.

- [11] Costa, Giuseppe. *Robust Controller of Gantry Crane*.1999.

- [12] R.C.Dorf, (1986). *Modern Control System*, fourth edition, Addison-Wesley.

- [13] Katsuhiko Ogata. *Modern Control Engineering*, second edition.

- [14] Inteco Ltd., "3D Crane", Jan 2006, <http://www.3DCrane.com>

APPENDICES

Appendix A: Milestone of Second semester of Final Year Project

Appendix B: MATLAB File for Simulation

Appendix C: Simulink Diagram for Model Verification

APPENDIX A
MILESTONE OF SECOND SEMESTER OF FINAL YEAR
PROJECT

TITLE: ANTI SWING CONTROLLER OF 3D CRANE

Work Program for January 2006 Semester (Final Year Project)

No	Detail / Work	2	3	4	5	6	7	8	9	10	11	12	13	14	15	19	20
1.	Laboratory experiment and testing	[Shaded]															
	-Final test and solution											[Shaded]					
2.	Reports																
	-Progress Report I			[1/2]													
	-Progress Report II						[2/3]										
	-Draft Report												[7/13]				
	-Final Report														[10/5]		
	-Technical Report																[12/6]
4.	Oral Presentation															[5/6-9/6]	

* Work programme schedule is subject to change

APPENDIX B
MATLAB FILE FOR CONTROLLER

```
A=[0 1 0 0; 0 -10.728 0.3383 0; 0 0 0 1; 0 21.46 -20.32 0];
B=[0;2.4138;0;-5.36];
C=[1 0 0 0;0 0 1 0];
D=[0;0];

%designing pole placement controller%
wn=1.6;
num=wn^2;
den=[1 1.4*wn wn^2];
g=tf(num,den);
des1=pole(g)
des=[des1' -15 -10]
k1=place(A,B,des)

%input reference%
TT=[A B;C D]
inv(TT)
N=inv(TT)*[zeros(1,length(A)) 1]';
Nx=N(1:end-1);
Nu=N(end);
Nbar=Nu+k1*Nx
sys1=ss(A-B*k1,B,C,D);
sys2=ss(A-B*k1,B*Nbar,C,D);
[y,t,x]=step(sys1,t);
plot(t,y)
[y2,t2,x2]=step(sys1,t);
plot(t2,y2)
```

```

%finding the new matrix%
a1=A-B*k1;
poles=eig(a1)
t=[0:.1:20];
u=[ones(size(t))];

%initial response%
sys=ss(A-B*k1, eye(4), eye(4), eye(4));

x=initial(sys,[1;0;0;0],t);
x1=[1 0 0 0]*x';
x2=[0 1 0 0]*x';
x3=[0 0 1 0]*x';
x4=[0 0 0 1]*x';

subplot(4,1,1);plot(t,x1),grid
title('Response to initial condition')
ylabel('state variable x1')

subplot(4,1,2);plot(t,x2),grid
ylabel('state varibale x2')

subplot(4,1,3);plot(t,x3),grid
ylabel('state varibale x3')

subplot(4,1,4);plot(t,x4),grid
xlabel('t(sec)')
ylabel('state varibale x4')

```

APPENDIX C

SIMULINK DIAGRAM FOR MODEL VERIFICATION

